7-16-2003

Evolution of Gases and Particles from a Savanna Fire in South Africa

Peter V. Hobbs
University of Washington - Seattle Campus

Parikhit Sinha
University of Washington - Seattle Campus

Robert J. Yokelson
University of Montana, Missoula

Ted J. Christian
University of Montana, Missoula

Donald R. Blake
University of California, Irvine

See next page for additional authors

Evolution of gases and particles from a savanna fire in South Africa

Peter V. Hobbs,[1] Parikhit Sinha,[1] Robert J. Yokelson,[2] Ted J. Christian,[2] Donald R. Blake,[3] Song Gao,[4] Thomas W. Kirchstetter,[5] Tica Novakov,[5] and Peter Pilewskie[6]

Received 21 March 2002; revised 24 June 2002; accepted 25 July 2002; published 8 March 2003.

[1] Airborne measurements of particles and gases from a 1000-ha savanna fire in South Africa are presented. These measurements represent the most extensive data set reported on the aging of biomass smoke. The measurements include total concentrations of particles (CN), particle sizes, particulate organic carbon and black carbon, light-scattering coefficients, downwelling UV fluxes, and mixing ratios for 42 trace gases and 7 particulate species. The ratios of excess nitrate, ozone, and gaseous acetic acid to excess CO increased significantly as the smoke aged over ~40–45 min, indicating that these species were formed by photochemistry in the plume. For 17 other species, the excess mixing ratio normalized by the excess mixing ratio of CO decreased significantly with smoke age. The relative rates of decrease for a number of chemical species imply that the average OH concentration in the plume was $\sim 1.7 \times 10^7$ molecules cm^{-3}. Excess CN, normalized by excess CO, decreased rapidly during the first ~5 min of aging, probably due to coagulation, and then increased, probably due to gas-to-particle conversion. The CO-normalized concentrations of particles <1.5 μm in diameter decreased, and particles >1.5 μm diameter increased, with smoke age. The spectral depletion of solar radiation by the smoke is depicted. The downwelling UV flux near the vertical center of the plume was about two-thirds of that near the top of the plume. *INDEX TERMS:* 0315 Atmospheric Composition and Structure: Biosphere/atmosphere interactions; 0317 Atmospheric Composition and Structure: Chemical kinetic and photochemical properties; 0322 Atmospheric Composition and Structure: Constituent sources and sinks; 0345 Atmospheric Composition and Structure: Pollution—urban and regional (0305); 3374 Meteorology and Atmospheric Dynamics: Tropical meteorology; *KEYWORDS:* gases, particles, biomass fires, smoke, savanna fires, evolution of smoke

Citation: Hobbs, P. V., P. Sinha, R. J. Yokelson, T. J. Christian, D. R. Blake, S. Gao, T. W. Kirchstetter, T. Novakov, and P. Pilewskie, Evolution of gases and particles from a savanna fire in South Africa, *J. Geophys. Res.*, *108*(D13), 8485, doi:10.1029/2002JD002352, 2003.

1. Introduction

[2] Biomass burning is a major source of atmospheric trace gases and particles [*Crutzen and Andreae*, 1990; *Fishman et al.*, 1991]. Savanna fires are the largest source of biomass burning emissions worldwide, and tropical Africa contains about two-thirds of the world's savanna [*Hao and Liu*, 1994]. Savanna burning emits a wide variety of species that influence global tropospheric chemistry, including carbon monoxide (CO), nitrogen oxides (NO_x), hydrocarbons, halocarbons, oxygenated organic compounds, and particles [*Crutzen and Andreae*, 1990; *Yokelson et al.*, 2003]. Smoke aerosols perturb atmospheric radiation through their effects on light extinction and cloud properties [e.g., *Hobbs and Radke*, 1969; *Eagan et al.*, 1974; *Hobbs et al.*, 1998; *Reid et al.*, 1999]. The photochemical oxidation of CO and organic compounds in the presence of NO_x in smoke produces ozone (O_3) [e.g., *Radke et al.*, 1978; *Goode et al.*, 2000]. Ozone and oxygenated compounds are key precursors of the hydroxyl radical (OH), which is the primary oxidant in the troposphere and is responsible for the removal of reactive pollutants released into the atmosphere by anthropogenic and natural processes [e.g., *Seinfeld and Pandis*, 1998].

[3] There is a growing body of information on initial emissions from biomass fires [e.g., *Stith et al.*, 1981; *Delmas*, 1982; *Radke et al.*, 1988; *Ward and Hardy*, 1991; *Hurst et al.*, 1994; *Andreae et al.*, 1996; *Ferek et al.*, 1998; *Sinha et al.*, 2003; *Yokelson et al.*, 2003], but less is known about the evolution of aging smoke. As smoke ages, it is diluted by mixing with the ambient air, which decreases the mixing ratios of most species emitted by the fire. In addition, some species in the smoke are consumed and others produced by photochemical reactions and other

[1]Department of Atmospheric Sciences, University of Washington, Seattle, Washington, USA.
[2]Department of Chemistry, University of Montana, Missoula, Montana, USA.
[3]Department of Chemistry, University of California, Irvine, California, USA.
[4]Department of Chemistry, University of Washington, Seattle, Washington, USA.
[5]Lawrence Berkeley National Laboratory, Berkeley, California, USA.
[6]NASA Ames Research Center, Moffett Field, California, USA.

0148-0227/03/2002JD002352

processes. Consequently, to assess the regional and global effects of smoke, and to evaluate plume models that include in situ chemical reactions and physical processes, measurements are needed to determine how aging affects the compositions, concentrations, and properties of species in smoke plumes from biomass burning. Changes in the concentrations of species due to in situ chemical and physical processes are revealed, in spite of simultaneous dilution due to mixing with the ambient air, by measuring the change in the ratio of the excess concentration of a species to that of a long-lived tracer for the smoke (such as CO or CO_2).

[4] *Radke et al.* [1988] compared measurements of light scattering and extinction in smoke above and downwind of a chaparral fire in California. *Liousse et al.* [1995] used ground-based Sun photometer measurements, and measurements of carbonaceous particles collected on filters, to infer that smoke aerosol from a savanna fire on the Ivory Coast underwent rapid transformations with aging.

[5] In studies of smoke from cerrado and rain forest regions of Brazil, *Reid et al.* [1998] found that the properties of aged gases and particles in regional hazes dominated by biomass burning were significantly different from those of young smoke. For example, as the smoke aged the excess nonmethane hydrocarbons ($C < 11$) ratioed to excess CO dropped by about one-third, and the aerosol mass to CO ratio increased by $\sim$20–40% with one-third to one-half of the mass growth likely occurring in the first few hours of aging. Changes in particle sizes and compositions during aging had a large impact on the optical properties of the aerosols.

[6] *Hobbs et al.* [1996] obtained airborne measurements in a smoke plume from a prescribed biomass burn on the Pacific coast of Washington State. Measurable decreases in the CO_2-normalized concentrations of NO and NO_x were documented over about 35 min of aging. In 1.8 h, the CO_2-normalized concentration of SO_2 decreased by about 60%, and the peak in the CO_2-normalized particle number concentration decreased dramatically while the particle number mode shifted from 0.16 to 0.28 μm and the particle volume mode from 0.25 to 0.38 μm. The mixing ratio of O_3 was below ambient very close to the fire, but it rose quickly and peaked after about a half-hour of aging. Using a high-resolution plume model, *Trentmann et al.* [2002] were able to reproduce some aspects of the physical evolution of the smoke described by Hobbs et al.

[7] *Goode et al.* [2000] reported that the ratio of excess O_3 to excess CO rose to as much as 8.9% within 2 h of aging near the top of an Alaskan smoke plume. On the same timescale, the ratio of excess NH_3 to excess CO fell by about two-thirds, and both formic and acetic acid doubled with respect to CO. These observations are mostly consistent with a photochemical model of a smoke plume developed by *Mason et al.* [2001], which includes oxygenated organic compounds. On longer timescales, measurements of excess O_3/excess CO have been reported for haze layers produced by biomass burning, the ages of which in days were estimated roughly [*Wofsy et al.*, 1992; *Andreae et al.*, 1994; *Mauzerall et al.*, 1996].

[8] In August and September 2000, the University of Washington (UW) Cloud and Aerosol Research Group (CARG), with its Convair-580 research aircraft, participated in the Southern African Regional Science Initiative 2000 (SAFARI 2000) field project. Since one of the goals of SAFARI 2000 is to study the emissions and transformations of smoke from biomass burning, we paid particular attention to obtaining detailed measurements of smoke from ten savanna fires in southern Africa. The measurements obtained in smoke immediately above these fires (i.e., "initial" smoke) are described by *Sinha et al.* [2003] and *Yokelson et al.* [2003]. In addition, measurements of particles and gases were made on smoke samples of known ages downwind of several savanna fires. In this paper we describe such measurements for a relatively large prescribed savanna fire that was ignited in the Timbavati game reserve in South Africa on 7 September 2000 (hereafter referred to as the Timbavati fire).

2. Instrumentation and Sampling Techniques

[9] All of the measurements described in this paper were obtained aboard the UW Convair-580 research aircraft. A complete list of the instruments aboard the aircraft is given by P. V. Hobbs in Appendix A of *Sinha et al.* [2003]. Brief information on each of the instruments used in the present study is given below.

2.1. Continuous Measurements

[10] Ambient air temperatures were measured with an in-house built temperature sensor enclosed in a reverse-flow housing to eliminate dynamic heating. Total temperature was measured with a Rosemount platinum resistance thermometer, and the ambient temperature derived from this by correcting for dynamic heating. The ambient dewpoint temperature, from which the ambient relative humidity (RH) could be derived, was measured with a Cambridge chilled-mirror device.

[11] The NASA Ames Solar Spectral Flux Radiometer (SSFR) was used to measure irradiance over the wavelength range 300–1700 nm [*Pilewskie et al.*, 2003]. Spectral resolution is 9 to 12 nm over the spectra range. The dynamic resolution is 15 bits full range. Integration time was nominally 100 ms and spectral sampling rate was approximately 1 Hz. The SSFR was calibrated for wavelength response, angular response, and absolute spectral power. The SSFR was calibrated before and after flights using a LI-COR field calibration unit, which allowed monitoring of the stability of the SSFR over the duration of the experiment. Absolute accuracy of spectral irradiance was estimated to be 3% across the spectrum. Precision was estimated to be 0.1% over one day and 1% over one month.

[12] Continuous measurements of sulfur dioxide (SO_2) concentrations were made with a Teco 43S pulsed fluorescence analyzer (precision 7%, detection limit 1 ppbv). A TSI 3025A ultrafine condensation particle counter was used to obtain continuous measurements in the smoke plume of the total concentrations of particles (CN), in the size range 0.003–3 μm diameter, with a precision of 10%. Continuous measurements of particle size spectra from 0.5 to 3.0 μm diameter were measured with a TSI 3320 aerodynamic particle sizer. The light-scattering coefficient of particles was measured continuously with an MS Electron nephelometer.

2.2. AFTIR

[13] An airborne Fourier transform infrared spectrometer (AFTIR) was used aboard the Convair-580 aircraft. The AFTIR had a dedicated inlet that directed ram air through a Pyrex multipass cell with an exchange time of 4–5 s. During plume penetrations, the AFTIR was used to grab smoke samples and to detain them for 2–3 min of signal averaging. This allowed measurements of the major reactive and stable trace gases present above 5–20 ppbv. The species measured were water vapor (H_2O), carbon dioxide (CO_2), CO, nitric oxide (NO), nitrogen dioxide (NO_2), methane (CH_4), ethene (C_2H_4), acetylene (C_2H_2), formaldehyde (HCHO), methanol (CH_3OH), acetic acid (CH_3COOH), formic acid (HCOOH), ammonia (NH_3), O_3, and hydrogen cyanide (HCN). The AFTIR technique, the precision of the measurements, and many of the results are discussed by *Yokelson et al.* [2003].

2.3. Filters and Electron Microscope Grids

[14] Particles were collected for specified time periods on quartz filters (Pallflex 2500 QAT-UP), Teflon filters (Gelman Sciences Teflo membrane, 2.0 μm pore size), and on electron microscope (EM) grids. The Teflon filters were weighed before and after particle sampling in a humidity and temperature controlled chamber (RH = 40%, T = 293 K) to determine the masses of dry total particulate matter (TPM) collected on the filters. From control and field blank filters, the uncertainty of the dry TPM was estimated to be ±6 μg. By comparison, the typical dry TPM loading for the smoke aerosol samples was always greater than 100 μg.

[15] After gravimetric analysis, the Teflon filters were extracted in deionized water (HPLC grade) and analyzed by a standard ion chromatography system. This analysis yielded mass concentrations of the chloride, nitrate and sulfate (Cl^-, NO_3^- and SO_4^{2-}, respectively) to a precision of 5%, as well as several organic species (precision within 20%) such as oxalate ($C_2O_4^{2-}$). An Inductively Coupled Plasma-Atomic Emission Spectrometer was used to measure the mass concentration of the potassium ion (K^+) to a precision of 4%. Each of these measurements was accompanied by field blanks to correct for background signals and to estimate measurement uncertainties and detection limits. Further details on the Teflon filter analyses, and results obtained are given by *Gao et al.* [2003].

[16] Aerosol samples collected intermittently on quartz (Pallflex 2500 QAT-UP) filters were used to determine the concentration of particulate carbon. The quartz filters were baked before use at 800°C for at least 6 h to remove carbonaceous impurities, and then analyzed for total carbon (TC) content using the evolved gas analysis (EGA) method described by *Novakov* [1981, 1982]. In EGA, a portion of the filter is heated at a constant rate (40°C min^{-1} in this case) from 50 to 800°C in an oxygen atmosphere. The carbon-containing gases that evolve from the sample are converted to CO_2 (over a manganese dioxide catalyst maintained at 800°C) that is subsequently measured with a nondispersive infrared analyzer (Beckman Model 870). A plot of the CO_2 concentration versus temperature is called a thermogram. The area under a thermogram is proportional to the TC content of the analyzed sample. The tandem filter method described by *Turpin et al.* [1994] and *Kirchstetter et al.* [2001] was used to adjust estimates of TC for the positive sampling artifact that results from the adsorption of organic gases on the quartz filters. Black carbon (BC) concentrations were estimated with an optical transmission technique similar to that described by *Rosen and Novakov* [1983]. This method compares the attenuation of white light through a loaded filter relative to that of a blank filter. The relationship between optical attenuation (ATN) and the BC concentration (μg cm^{-2}) is given by $ATN = \sigma \cdot BC$, where $ATN = 100\ln(I_o/I)$, and I_o and I are the transmitted light intensities through the blank and loaded filters, respectively, and σ is the mass absorption cross section for BC deposited on quartz (m^2 g^{-1}) [*Gundel et al.*, 1984]. A value of 20 m^2g^{-1} was used for the mass absorption cross section. This value was derived from comparison of light absorption measurements and BC concentrations (measured by thermal EGA) on many samples [*Gundel et al.*, 1984; *Kirchstetter et al.*, 2003]. Further information on the EGA and optical transmission techniques used here, and the results obtained, are given by *Kirchstetter et al.* [2003].

[17] Since the time that it took the aircraft to cross the width of a smoke plume (~1–2 min) was too short to pass enough smoke through the Teflon filters, quartz filters, and the EM grids for subsequent detailed analyses of the aerosol, a "grab-bag" technique was used. The grab-bag consisted of a 2.5 m^3 electrically conducting plastic (Velostat) bag, which could be filled with a sample of smoke in 12 s when exposed to ram air. The sample in the grab-bag was drawn through the various gas and aerosol measuring instruments aboard the aircraft, through the filters, and onto the EM grids, for subsequent analysis. Particle size measurements could also be made using the bag samples. The grab-bag system had an aerosol 50% cut-off diameter of about 4 μm, as larger particles were lost in the inlet and on the walls of the grab bag. When crossing a plume, the grab-bag was also used to obtain samples for SO_2 measurements using the Teco 43S pulsed fluorescence analyzer. Grab-bag samples were followed by sampling of the ambient air, allowing determination of excess concentrations of species in a plume.

2.4. Canister Samples

[18] Electropolished stainless steel canisters were filled with air samples from smoke plumes, and ambient air just upwind of the fires, using a stainless steel inlet that passed through the aircraft fuselage. The canister samples coincided with the "grab-bag" samples. A typical sampling time for a canister was 30 s. The canister samples were subsequently analyzed for hydrocarbons, halocarbons, dimethyl sulfide (DMS), and methyl nitrate (CH_3ONO_2).

[19] For each canister sample, mixing ratios of C_2–C_9 nonmethane hydrocarbons (NMHC), methyl chloride (CH_3Cl), methyl iodide (CH_3I), chloroform ($CHCl_3$), methyl bromide (CH_3Br), bromoform ($CHBr_3$), chlorofluorocarbons (CFCs), hydrochlorofluorocarbons (HCFCs) and hydrofluorocarbons (HFCs) were determined by gas chromatography with flame ionization, electron capture and mass spectrometer detection. The precision of the NMHC, $CHCl_3$, $CHBr_3$ and methyl halide measurements was 3%, and the NMHC detection limit was 3 pptv.

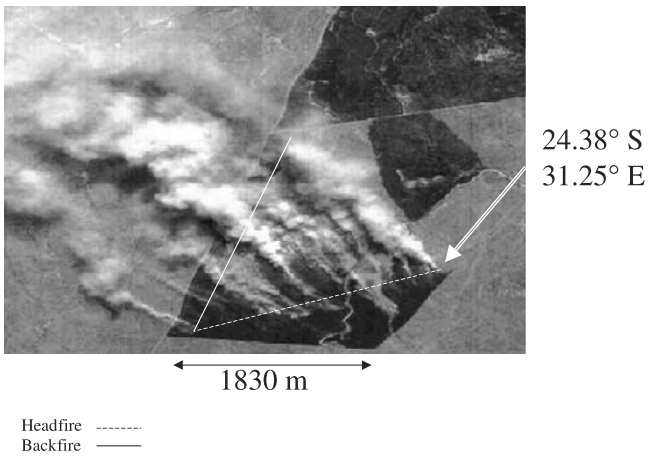

Figure 1. Nadir-viewing image at 0829 UTC on 7 September 2000 of the prescribed fire in the Timbavati Private Game Reserve obtained from AirMISR aboard the NASA ER-2 aircraft. The image is a composite constructed from red (672 nm), green (558 nm), and blue (446 nm) bands. See color version of this figure at back of this issue.

Measurements of the longer-lived CFCs, HCFCs, and HFCs were precise to within 1%. Mixing ratios (precisions in parentheses) of CO_2 (3%), CO (5%), and CH_4 (0.1%) were determined using separate instrumentation. A detailed description of the analytical procedure for the canister samples, including quantification of the measurement precision for individual compounds, is given by *Colman et al.* [2001].

3. Definitions of Excess Molar Mixing Ratio, Normalized Excess Molar Mixing Ratio, and Combustion Efficiency

[20] The excess molar (or volume) mixing ratio, ΔX, of a species X in a smoke plume is defined as:

$$\Delta X = X_{plume} - X_{ambient} \quad (1)$$

where, X_{plume} and $X_{ambient}$ are the molar (or volume) mixing ratios of X in the smoke plume and in the ambient air, respectively.

[21] The normalized excess molar mixing ratio of a species X is the excess molar mixing ratio of X in the smoke divided by the excess molar mixing ratio of a simultaneously measured reference gas (such as CO or CO_2). For example, a normalized excess molar emission ratio of species X relative to CO is $\Delta X/\Delta CO$. It is common to refer to this as the excess molar emission ratio. However, we prefer to use this wording only when ΔX and ΔCO are measured very close to a fire, as described by *Sinha et al.* [2003]. Since CO is a biomass burning product with a lifetime of $\sim$1 month in the ambient, tropical troposphere, most of the decrease in the excess molar mixing ratio of CO in the smoke plume, at least in the first few hours, is due to mixing with the ambient air. Therefore, by dividing ΔX by ΔCO, the effects of dilution of ΔX due to mixing with the ambient air are largely removed, so that other physical and chemical processes that change ΔX in the plume can be isolated.

[22] The combustion efficiency (CE) is the molar ratio of excess carbon (C) emitted as CO_2 from a fire to the total excess carbon emitted [*Ward and Hardy*, 1991]:

$$CE = \frac{\Delta C_{CO_2}}{\Delta C_{CO_2} + \Delta C_{CO} + \Delta C_{CH_4} + \Delta C_{NMOC} + \Delta C_{PC}} \quad (2)$$

where NMOC and PC indicate nonmethane organic compounds and particulate carbon, respectively. Thus, CE is the fraction of fuel carbon emitted that is completely oxidized to CO_2.

[23] Although CE is a useful quantity for fire models, it is often difficult to measure all of the individual carbon species in the emissions from a fire. As will be shown below, the emission of CO is closely linked to the emission of CH_4, NMOC, and PC. Therefore, in this study we have chosen to use the modified combustion efficiency (MCE) as the principal quantity to describe the relative amounts of flaming and smoldering combustion [*Ward and Hao*, 1992; *Ward and Radke*, 1993], which is defined as:

$$MCE = \frac{\Delta C_{CO_2}}{\Delta C_{CO_2} + \Delta C_{CO}} \quad (3)$$

Since CH_4, NMOC, and PC are emitted in small quantities relative to CO_2 and CO, the difference between CE and MCE is typically only a few percent.

[24] Both CE and MCE are useful as indicators of the relative amounts of flaming and smoldering combustion that generate emissions. In laboratory studies, *Yokelson et al.* [1996] found that pure flaming combustion has an MCE near 0.99 and pure smoldering combustion an MCE near 0.8. Therefore, an MCE <0.9 roughly indicates >50% smoldering combustion, and an MCE >0.9 suggests >50% flaming combustion.

4. Vegetation and Fire

[25] The Timbavati fire was a carefully controlled and monitored fire in the lowveld of South Africa (T. Land-

Figure 2. Photograph of the Timbavati fire taken at 0836 UTC on 7 September 2000 from the Convair-580 aircraft. (Photo: P. V. Hobbs). See color version of this figure at back of this issue.

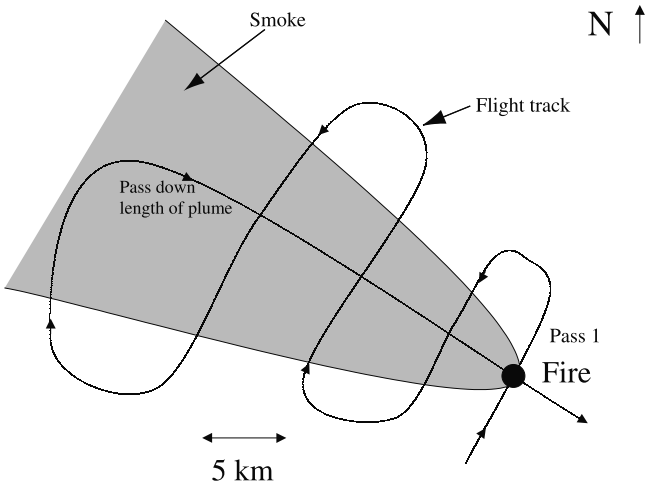

Figure 3. Simplified schematic of the Convair-580 flight track in the smoke plume from the Timbavati fire.

mann, personal communication, 2002). In this region of the lowveld the vegetation varies from south Zambezian undifferentiated woodland to Tongaland-Pondoland bushland [*White*, 1981, 1983]. The fuel for the Timbavati fire was mainly grass, with litter (leaves and twigs) constituting only about 1% of the fuel. The fuel load was ~4800 kg/ha and ~1000 ha were ignited. Since ~80% of the fuel exposed to fire was combusted, $\sim 3.8 \times 10^6$ kg of biomass was burned (T. Landmann, personal communication, 2002). The fire was ~2 km in width.

[26] The main fire was ignited at 0801 UTC (1001 local time) and the flames reached ~2 m in height. A downwind backfire ignited at 0730 UTC had flames that reached ~0.3–0.5 m in height. Prior to 1100 UTC the fire was predominantly flaming; thereafter, smoldering combustion dominated. The fire was extinct by 1130 UTC, after smoldering samples of wood were put out near the edge of the plot.

[27] Figure 1 shows an image of the fire taken at 0829 UTC from the NASA ER-2 aircraft flying at an altitude of ~20 km. The locations of the head fire, back fire, and the ignition point can be seen in Figure 1. Figure 2 shows a photograph of the fire 7 min later, which was taken from the Convair-580 as it approached the fire from upwind.

5. Flight Track

[28] Measurements of the smoke from the Timbavati fire were acquired aboard the Convair-580 from 0842 to 1036 UTC, which was during the predominantly flaming stage of the fire. Figure 3 shows a simplified schematic of the flight track of the Convair-580 during this period. From about 0842 to 1036 UTC samples of smoke were obtained in a series of passes perpendicular to the axis of the plume at various distances and altitudes downwind of the head fire. During these passes, the pilot was instructed to fly the aircraft across the width of the plume.

[29] Table 1 summarizes the times and locations of the plume samples, and some of the parameters measured. Using the average wind speed measured aboard the aircraft (11.3 ± 0.9 m s^{-1}), and the distances downwind from the

Table 1. Samples of Smoke From the Timbavati Fire Obtained From the Convair-580[a]

Sample	Time, UTC	Latitude, °S	Longitude, °E	Distance From Head Fire, km	Altitude, m	Age of Smoke, min[b]	Pressure, hPa	Temperature, °C	Relative Humidity, %	Modified Combustion Efficiency, MCE	Downwelling Ultraviolet (300–390 nm) Flux in Plume, W m^{-2}	Upwelling Ultraviolet (300–390 nm) Flux in Plume, W m^{-2}
1	0843	24.37	31.22	1.0	598	1	941	19	35	0.94	37	2.1
2	0857	24.36	31.25	0.2	564	0	942	19	34	0.93	14	2.3
3	0923	24.33	31.25	4.9	896	7 ± 1	909	16	40	0.92	25	3.5
4	0939	24.18	31.12	20.8	1440	31 ± 3	848	14	78	0.91	42	8.3
5	1014	24.16	31.17	26.2	545	39 ± 4	952	21	34	0.93	29	2.3
a	0843	24.37	31.26	1.7	616	3	939	21	38	0.93	26	2.2
b	0846	24.37	31.24	0.1	739	0	920	20	36	0.94	40	3.0
c	0855	24.29	31.27	9.5	710	14 ± 1	942	20	34	0.91	33	2.5
d	0921	24.36	31.23	1.9	862	3	903	17	41	0.88	28	2.8
e	0933	24.24	31.28	15.7	1710	23 ± 2	843	16	22	0.93	45	4.7
f	0934	24.21	31.21	17.7	1430	26 ± 3	849	14	32	0.93	44	8.4
g	0940	24.19	31.21	19.9	1440	29 ± 3	846	15	78	0.91	42	8.3
h	0946	24.36	31.25	2.0	564	3	940	21	35	0.91	29	1.5
i	1015	24.18	31.09	26.6	545	39 ± 4	943	22	34	0.92	29	2.3
j	1021	24.17	31.09	27.3	500	40 ± 4	956	23	32	0.91	24	1.6
k	1036	24.15	31.08	30.1	538	44 ± 4	945	23	28	0.94	32	2.4

[a]Samples 1–5 were collected in canisters and analyzed by gas chromatography. Samples a–k were measured by AFTIR.
[b]Derived from an average measured wind speed of 11.3 ± 0.9 m s^{-1}.

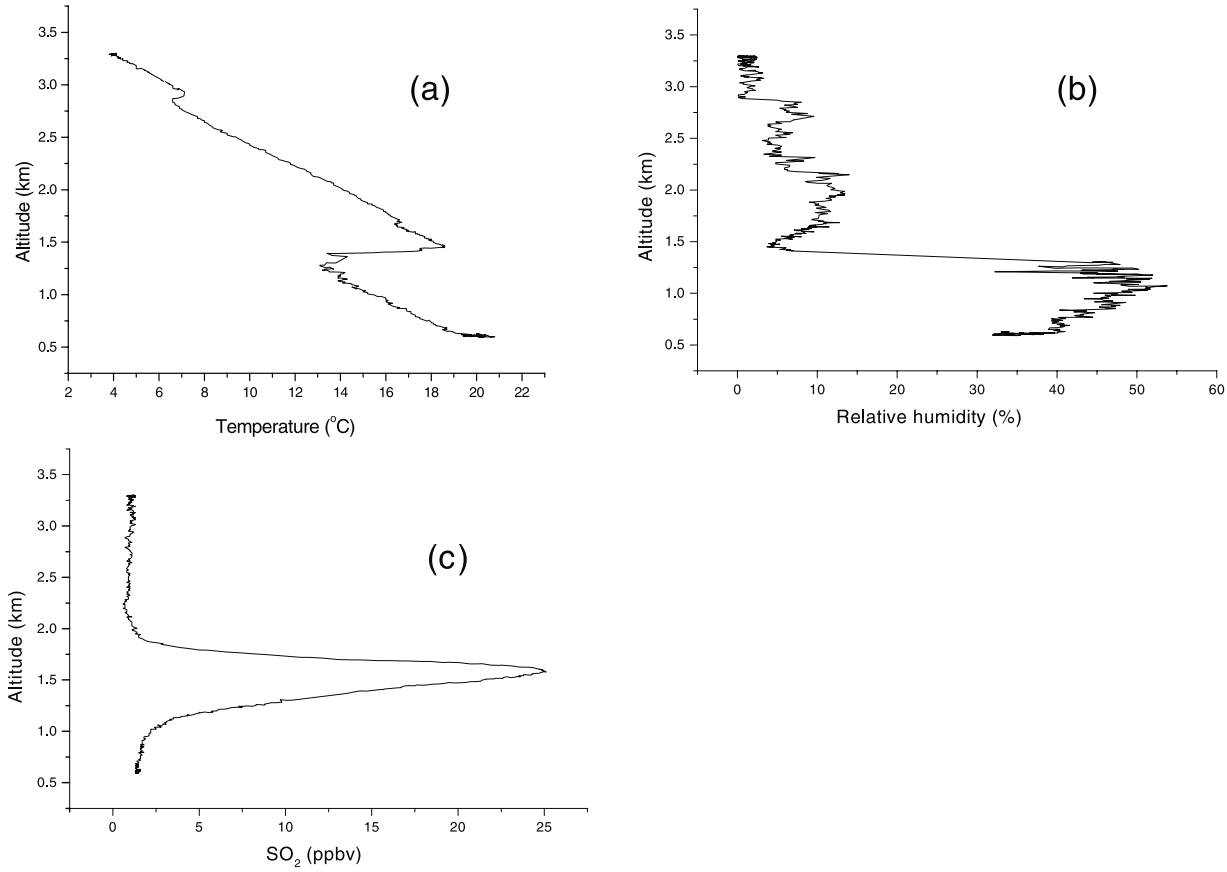

Figure 4. Vertical profiles of temperature, relative humidity, and SO_2 concentration measured upwind of the Timbavati fire from 0829 to 0840 UTC.

head fire of the various samples, the age of the smoke in each sample was estimated (see Table 1). Environmental conditions for each sample (e.g., pressure, temperature, RH, UV flux, etc.) are also given in Table 1. Samples 1–5 in Table 1 were collected in stainless steel canisters and on Teflon and quartz filters. Samples a–k in Table 1 were analyzed by AFTIR.

[30] The time interval between crossing the plume ~0.1 km and 30.1 km downwind of the head fire was 110 min. Therefore, the average speed of the aircraft along the length of the plume was 4.5 m s^{-1}, compared to the average wind speed of 11.3 ± 0.9 m s^{-1}. Hence, the first and last samples were not exactly Lagrangian pairs. However, as mentioned previously, the fire was predominantly flaming and moving into fresh fuel during this period of time (as indicated also by the MCE values in Table 1). Therefore, variations in the excess mixing ratio of a species with age of the smoke should primarily reflect effects that occurred downwind.

6. Results and Discussion

6.1. Vertical Profiles Upwind of the Fire and Transects Through the Smoke Plume

[31] Figure 4 shows vertical profiles of temperature, relative humidity, and SO_2 concentration measured from 0829 to 0840 UTC just upwind of the Timbavati fire. The strong temperature inversion at ~1.3 km (Figure 4a) produced a peak in the SO_2 concentration at this level (Figure 4c).

[32] Shown in Figures 5 and 6 are the light-scattering coefficient due to particles and CN concentrations measured in horizontal tracks across the width of the smoke plume and at various distances downwind of the fire. At 0.2 km downwind, where the width of the plume was ~3–4 km, the peak values of the light-scattering coefficient and CN were ~0.0022 m^{-1} and ~7 × 10^5 cm^{-3}, respectively. The

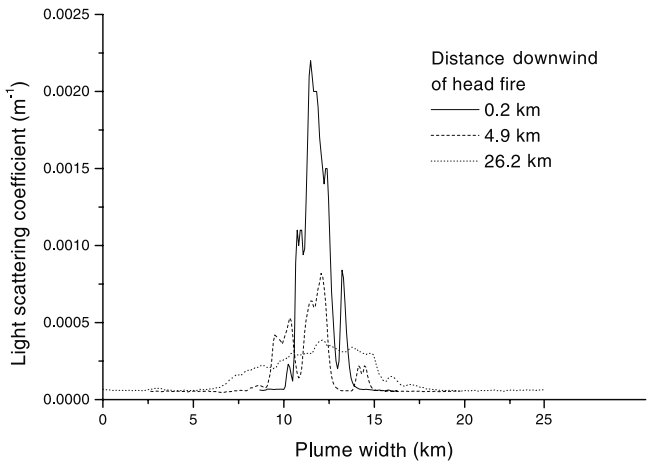

Figure 5. Particle light-scattering coefficient across the width of the Timbavati smoke plume at various distances downwind of the fire.

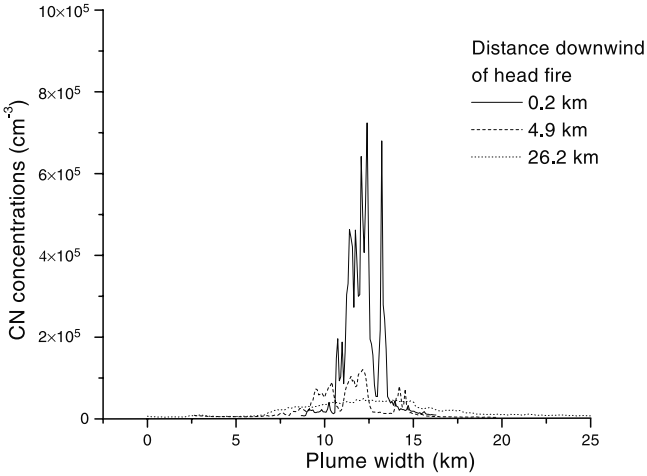

Figure 6. Condensation nucleus (CN) concentrations across the width of the Timbavati smoke plume at various distances downwind of the fire.

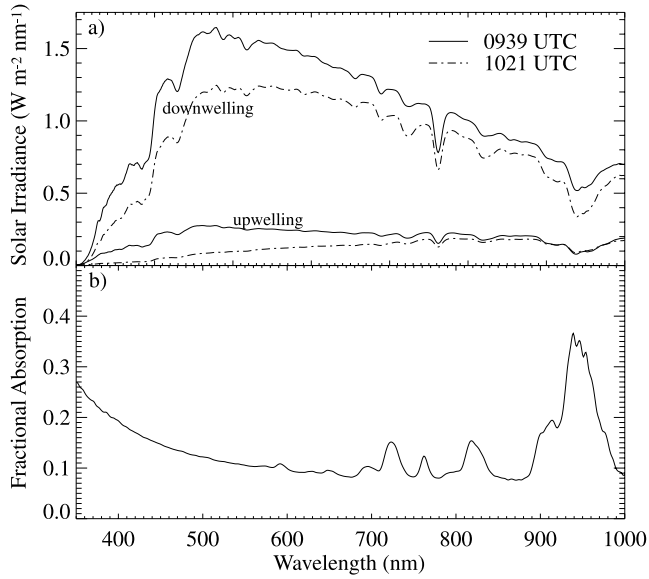

Figure 8. (a) Upwelling and downwelling spectral irradiance 20–25 km downwind of the Timbavati fire. The solid curve was obtained at 0939 UTC near plume top, and the dashed curve at 1021 UTC at ~1000 m below plume top. (b) Fractional absorption between plume top and ~1000 m below plume top.

corresponding values at 26.2 km downwind, where the width of the plume was ~10–15 km, were ~0.0004 m^{-1} and ~0.5×10^5 cm^{-3}.

6.2. Attenuation of Solar Radiation by Smoke

[33] Since photochemical reactions in the smoke will depend on the intensity of UV radiation, we show in Figure 7 the downwelling UV irradiance in the wavelength band 300–390 nm, measured by the SSFR aboard the Convair-580, in the Timbavati plume from 0842 to 1036 UTC. Generally, the aircraft was flown at about the vertical center of the plume, but for a brief period of time it was near the top of the plume. Near the center of the plume, the UV flux was about two-thirds of that near the top of the plume.

[34] Figure 8a shows SSFR-measured upwelling and downwelling irradiance spectra at 0939 UTC (solid curve) and at 1021 UTC (dashed curve), near plume top and approximately 1000 m below plume top, respectively. Both sets of measurements were obtained 20–25 km downwind of the fire. Figure 8b shows the fractional absorption (obtained by normalizing the absorbed solar radiation in

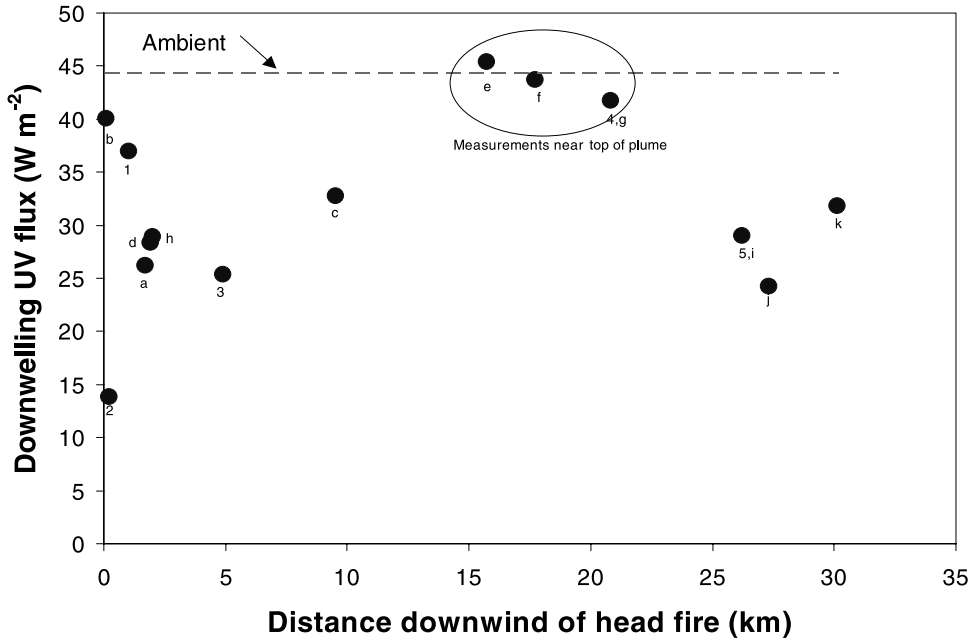

Figure 7. Downwelling UV irradiance from 300 to 390 nm measured along the length of the Timbavati smoke plume. The numbers and letters alongside each data point correspond to those given in the first column of Table 1.

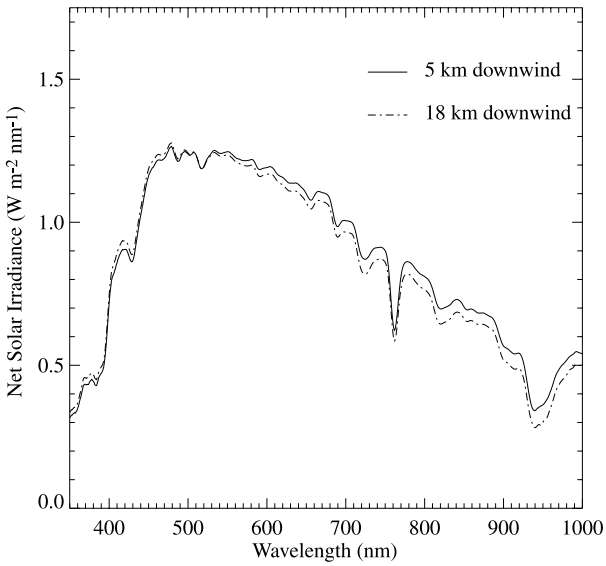

Figure 9. Net spectral irradiance in the smoke at 5 km and 18 km downwind of the Timbavati fire. Both measurement sets were made between ~750 and 1000 m below plume top.

the layer by the solar radiation incident at the top of the layer) in the 1000 m thick smoke layer. The smooth continuum-type absorption is due to the smoke particles; water vapor absorption is evident in the band centered at 940 nm as well as several other smaller bands in the near-infrared. Absolute layer absorption by the smoke was ~91 W m^{-2}, producing an instantaneous heating rate of ~7.4 K day^{-1}.

[35] The spectral behavior of the scattering and absorption by the smoke is similar to that reported by *Pilewskie et al.* [2003] and *Bergstrom et al.* [2003] and is consistent with absorption by elemental carbon [see *Bergstrom et al.*, 2002]. The aerosol single-scattering albedo decreased with increasing wavelength from the near-ultraviolet to near-infrared, but total layer absorption was greatest in the ultraviolet because of the increase in aerosol optical thickness with decreasing wavelength.

[36] We examined the spectral distribution of scattered solar irradiance with plume evolution by comparing spectral irradiance at various distances from the head fire. Figure 9 shows the average net solar irradiance (defined as the difference between downwelling and upwelling irradiance) at 5 km and 18 km downwind of the Timbavati fire, at approximately 750 to 1000 m below plume top. In the near-ultraviolet and visible part of the spectrum, where the greatest amount of absorption occurred, the net spectral irradiance is nearly identical at the two distances downwind. The only significant differences occurred in the far visible and near-infrared, which we attribute to changes in surface albedo. Thus, the radiation available to drive photochemical reactions had nearly the same spectral distribution, and was of similar magnitude, 5 km and 18 km downwind of the Timbavati fire.

6.3. Transformations of Chemical Species in the Plume

6.3.1. Effects of Dilution on Mixing Ratios

[37] Table 2 shows mixing ratios of the gases, particulate matter and ions that were measured in the Timbavati plume by gas chromatography (GC/C) and filters (F/GB) and which were considered to derive from biomass burning by the significant correlation of their excess mixing ratios with the excess mixing ratio of CO or CO_2 ($r^2 \geq 0.5$). Table 3 lists the excess mixing ratios of gases measured in the smoke plume by AFTIR.

[38] It can be seen from Tables 2 and 3 that the mixing ratios of many chemical species in the plume changed with distance from the fire. This could be due to chemical reactions, which may produce or consume a species with time. However, even for a species that is not affected by chemical reactions, the mixing ratio in the plume will generally decrease with increasing distance from a fire due to mixing of the smoke with the ambient air. As discussed in section 3, the dilution of a species due to mixing with the ambient air can be removed in large part, at least for the first few hours of travel, by dividing the excess molar mixing ratio of the species by the excess molar mixing ratio of CO.

[39] Isoprene has a daytime lifetime in the ambient tropical atmosphere of only ~60 min due to its reaction with OH [*Mauzerall et al.*, 1998]. Consequently, decreases in the excess mixing ratios of isoprene in young smoke should reflect both its reaction with OH and dilution due to mixing with ambient air. Figure 10 shows Δisoprene and Δisoprene/ΔCO as a function of the age of the smoke in the Timbavati plume. Both quantities decline to ambient levels at approximately the same rate, which indicates that chemical reactions were dominant in decreasing the concentration of isoprene in the plume.

[40] Figure 11 shows a plot similar to Figure 10 but for ethene, which has a significantly longer lifetime than isoprene. In this case, $\Delta C_2H_4/\Delta CO$ decreases only slightly with age (over ~40 min), but ΔC_2H_4 ratio falls off more rapidly (due to mixing with the ambient air).

6.3.2. Photochemistry

[41] A value of $\Delta X/\Delta CO$ measured before any significant postemission transformations is the emission ratio of compound X for the fire. Changes in $\Delta X/\Delta CO$ as smoke ages reveal the rate of photochemical and heterogeneous processes in the plume. Tables 4 and 5 show $\Delta X/\Delta CO$ values for many samples of various ages in the smoke from the Timbavati fire. While $\Delta X/\Delta CO$ decreases with the age of the smoke for various hydrocarbons, due to reactions with OH (or more slowly with O_3), it should increase for photochemical products. For example, Figure 12 shows $\Delta X/\Delta CO$ for acetic acid (CH_3COOH), O_3, and nitrate increasing as the smoke ages. After 40 min of aging, $\Delta CH_3COOH/\Delta CO$ is about three times its initial value (Figure 12a). By contrast, it took >2 h for this ratio to double in Alaskan smoke plumes [*Goode et al.*, 2000].

[42] In minutes-old smoke from the Timbavati fire the O_3 mixing ratio was below ambient due to reaction with NO and particles, but $\Delta O_3/\Delta CO$ rose to as much as 9% within 30 min (Figure 12b). In comparison, $\Delta O_3/\Delta CO$ rose more slowly to only ~1.5% in 30 min in a smoke plume in the Pacific Northwest of the United States [*Hobbs et al.*, 1996], and required ~2 h to reach 9% in an Alaskan smoke plume [*Goode et al.*, 2000]. These initial bursts of O_3 production may account for a significant portion of the total O_3 production in smoke plumes, since *Yokelson et al.* [2003] report $\Delta O_3/\Delta CO$ of 22% in biomass burning haze several

Table 2. Mixing Ratios of Gases and Mass Concentrations of Particles and Ionic Species in Samples 1–5 Listed in Table 1 and in the Ambient Air[a]

Species	Technique Used for Measurement[b]	Sample 2	Sample 1	Sample 3	Sample 4	Sample 5	Ambient Air
		Gases, ppbv					
Carbon dioxide (CO_2)	GC/C	425,000	427,000	391,000	397,000	388,000	377,000
Carbon monoxide (CO)	GC/C	3900	3500	1500	2300	1100	220
Sulfur dioxide (SO_2)	Teco 43S[c]	25	66	15	9.4	8.9	1.7
Methane (CH_4)	GC/C	1900	1870	1790	1820	1780	1740
Dimethyl sulfide (CH_3SCH_3)	GC/C	0.044	0.028	0.012	0.014	0.0051	bdl
Methyl bromide (CH_3Br)	GC/C	0.034	0.030	0.019	0.023	0.014	0.0096
Methyl chloride (CH_3Cl)	GC/C	3.4	3.0	1.7	2.1	1.2	0.68
Methyl iodide (CH_3I)	GC/C	0.0063	0.0054	0.0026	0.0035	0.0019	0.00064
Methyl nitrate (CH_3ONO_2)	GC/C	0.018	0.018	0.013	0.0225	0.0089	0.0057
Ethane (C_2H_6)	GC/C	13	9.8	4.3	7.2	3.3	0.86
Ethene (C_2H_4)	GC/C	35	32	12	16	6.0	0.32
Propane (C_3H_8)	GC/C	2.3	1.6	0.72	1.2	0.55	0.11
Propene (C_3H_6)	GC/C	8.8	7.4	2.6	2.3	0.83	0.031
Acetylene (C_2H_2)	GC/C	12	12	4.8	7.3	3.1	0.49
i-butane (C_4H_{10})	GC/C	0.18	0.14	0.054	0.084	0.044	0.009
n-butane (C_4H_{10})	GC/C	0.47	0.36	0.15	0.24	0.11	0.023
t-2-butene (C_4H_8)	GC/C	0.42	0.31	0.079	0.097	0.005	bdl
1-butene (C_4H_8)	GC/C	1.3	1.0	0.35	0.27	0.097	0.023
c-2-butene (C_4H_8)	GC/C	0.31	0.23	0.063	0.055	0.0060	bdl
i-pentane (C_5H_{12})	GC/C	0.053	0.037	0.019	0.030	0.012	0.006
n-pentane (C_5H_{12})	GC/C	0.11	0.082	0.037	0.061	0.026	0.009
1,3-butadiene (C_4H_6)	GC/C	1.4	1.2	0.38	0.086	0.033	bdl
3-methyl-1-butene (C_5H_{10})	GC/C	0.13	0.11	0.036	0.030	0.010	bdl
t-2-pentene (C_5H_{10})	GC/C	0.11	0.084	0.023	bdl	bdl	bdl
2-methyl-2-butene (C_5H_{10})	GC/C	0.12	0.089	0.019	bdl	bdl	bdl
2-methyl-1-butene (C_5H_{10})	GC/C	0.13	0.11	0.031	0.013	0.005	bdl
c-2-pentene (C_5H_{10})	GC/C	0.067	0.052	0.014	bdl	bdl	bdl
n-hexane (C_6H_{14})	GC/C	0.22	0.19	0.067	0.067	0.027	0.007
Isoprene (C_5H_8)	GC/C	0.79	0.64	0.15	0.018	0.015	0.018
2-methyl-1-pentene (C_6H_{12})	GC/C	0.078	0.056	0.016	bdl	bdl	bdl
Heptane (C_7H_{16})	GC/C	0.12	0.074	0.026	0.022	0.01	0.014
Benzene (C_6H_6)	GC/C	3.7	3.1	1.2	1.8	0.73	0.096
Toluene (C_7H_8)	GC/C	3.1	2.2	0.89	1.4	0.47	0.082
		Particulates, μg m^{-3}					
Total particulate matter (TPM)	F/GB	-	1180	282	-	179	30.1
Organic carbon (OC)	F/GB	-	206	57	-	34	3.6
Black carbon (BC)	F/GB	-	35.0	7.7	-	6.7	0.5
Chloride (Cl^-)	F/GB	-	193	28	-	5.4	bdl
Nitrate (NO_3^-)	F/GB	-	13.6	7.2	-	9.1	0.78
Sulfate (SO_4^{2-})	F/GB	-	25.0	9.2	-	8.1	1.2
Potassium (K^+)	F/GB	-	70.9	9.5	-	3.8	0.74

[a]The samples are listed in order of increasing distance from the fire. The measurements were obtained by gas chromatography. bdl indicates that the species was below the detection limit; dashes indicate no data.
[b]GC= gas chromatography via canisters; F/GB = filters via grab bag.
[c]Via grab bag.

Table 3. Excess Mixing Ratios (Δppbv) of Some of the Chemical Species Measured by AFTIR in Samples (a) Through (k) in Table 1

Species	Sample b	a	d	h	c	e	f	g	i	j	k
Carbon dioxide (CO_2)	68,600	79,200	6900	15,600	19,100	13,900	21,300	10,100	6100	6300	7100
Carbon monoxide (CO)	4024	5738	911	1592	1776	1042	1625	954	549	644	426
Methane (CH_4)	214	345	80	67	109	55	117	60	33	28	21
Ethene (C_2H_4)	58	91	12	20	21	bdl	bdl	bdl	bdl	bdl	bdl
Acetylene (C_2H_2)	14	19	bdl	bdl	6	bdl	bdl	bdl	bdl	bdl	bdl
Formaldehyde (HCHO)	74	109	20	25	16	31	37	31	10	10	20
Methanol (CH_3OH)	55	86	20	19	28	10	bdl	7	bdl	9	5
Acetic Acid (CH_3COOH)	58	75	23	53	14	30	71	36	27	35	32
Formic Acid (HCOOH)	33	33	bdl	6	17	11	bdl	5	bdl	bdl	bdl
Ammonia (NH_3)	13	5	bdl	3	bdl	bdl	bdl	bdl	bdl	bdl	bdl
Nitric oxide (NO)	52	57	bdl	bdl	bdl	bdl	bdl	bdl	bdl	bdl	bdl
Nitrogen dioxide (NO_2)	123	137	bdl	51	51	bdl	bdl	bdl	6	bdl	bdl
Hydrogen cyanide (HCN)	29	37	9	bdl	18	8	18	11	bdl	bdl	bdl
Ozone (O_3)	−52	−52	−12	bdl	22	60	98	86	31	54	19

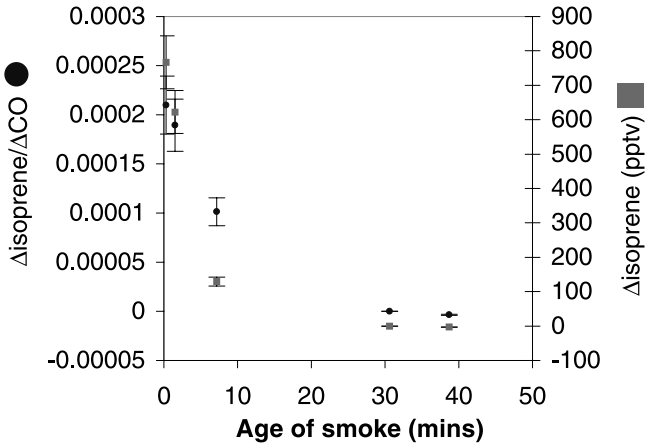

Figure 10. Excess volume mixing ratio of isoprene (squares), and the excess volume mixing ratio of isoprene normalized with respect to CO (circles), versus age of the smoke in the Timbavati plume.

days old off the coast of Namibia, and *Andreae et al.* [1994] measured a range of $\Delta O_3/\Delta CO$ values from 20% to 88% in biomass burning haze estimated to be about 10 days old over the South Atlantic Ocean. Hence, for some species $\Delta X/\Delta CO$ can increase significantly after emission, but the rate of change depends on the species and on local conditions. As expected, faster photochemistry is observed in subtropical Africa than at higher latitudes. Photochemistry should be faster near the top of a plume where ultraviolet light is more intense. The $\Delta O_3/\Delta CO$ values we measured high in the Timbavati plume (i.e., samples e, f and g in Figure 7) lie above the slope in Figure 12b that gives the average formation rate.

[43] Listed in Table 6, and shown in Figures 12–15, are those gases for which $\Delta X/\Delta CO$ either increased or decreased significantly with aging when modeled as a linear process. ("Significant" refers to a statistical confidence level of at least 95%.) Most of the hydrocarbons in Table 6 are alkenes, which react quickly with OH and more slowly with O_3. The oxidation of these hydrocarbons (and other organics, including those entrained in the plume) can lead to the formation of acetic acid, which increased significantly in the aged smoke (Table 6 and Figure 12a). The fates of several other species listed in Table 6 are similarly linked. For example, photolysis of NO_2 yields O_3. Thus, Table 6 shows that $\Delta NO_2/\Delta CO$ decreased while $\Delta O_3/\Delta CO$ increased. The ratio $\Delta NO_2/\Delta CO$ decreased to roughly one-third of its initial value in ~40 min. However, this measurement should not be viewed as quantitative, since all of the downwind NO_2 mixing ratios were near or below the detection limit of the AFTIR. Nitrogen dioxide can also react with OH to yield gas phase HNO_3, which can then be converted to particulate nitrate; $\Delta NO_3^-/\Delta CO$ increased by a factor of 2.5 in 39 min in the Timbavati plume.

6.3.3. Estimates of OH Concentrations in the Smoke

[44] The rate-limiting step for loss of many chemical species in the atmosphere is reaction with the OH radical. We can use this fact to estimate the average concentration of OH in the relatively young smoke from the Timbavati fire.

[45] If the rate of decrease in the CO-normalized excess mixing ratio of species X in a smoke plume is dominated by its reaction with OH, we can write:

$$\left(\frac{\Delta X}{\Delta CO}\right)_t = \left(\frac{\Delta X}{\Delta CO}\right)_0 \exp\{-k_x[OH]t\} \quad (4)$$

where $(\Delta X/\Delta CO)_0$ and $((\Delta X/\Delta CO)_t$ are the CO-normalized excess mixing ratios of X immediately over the fire (t = 0) and after the smoke has aged for time t, respectively, and k_x is the rate coefficient for X reacting with OH. If equation (4) is applied to two species X_1 and X_2, the following is obtained:

$$\ln\left(\frac{\Delta X_1}{\Delta X_2}\right)_t = -[OH](k_1 - k_2)t + \ln\left(\frac{\Delta X_1}{\Delta X_2}\right)_0 \quad (5)$$

where, k_1 and k_2 are the rate coefficients for X_1 and X_2, respectively, reacting with OH. Hence, a plot of $\ln(\Delta X_1/\Delta X_2)_t$ versus $(k_1 - k_2)t$ will have slope $-[OH]$, where [OH] is the average concentration of OH in the smoke as it ages over the time interval t.

[46] Results for the average OH concentrations derived in this way using combinations of the five best species (propene, ethene, 1-butene, ethane and CO) that have various reaction rates with OH but negligible competing loss rates due to O_3, are shown in Table 7; example plots are shown in Figure 16. The average derived concentration of OH, using room temperature rate constants, during the first ~40 min in the Timbavati plume is $(1.7 \pm 0.2) \times 10^7$ molecules cm^{-3}.

[47] Noontime, cloud-free, surface OH concentrations at the latitude and in the season of this study were modeled to be only $(3–4) \times 10^6$ molecules cm^{-3} [*Logan et al.*, 1981], or ~4–6 times lower than our estimated value for the OH concentrations in the Timbavati plume. Other models and measurements (including those of polluted urban air) yield maximum OH concentrations ranging from $\sim(2–10) \times 10^6$ molecules cm^{-3} [*Finlayson-Pitts and Pitts*, 2000]. The photochemical model of a smoke plume developed by *Mason et al.* [2001] predicts OH levels a little greater than 1×10^7 molecules cm^{-3} during the first hour of plume evolution when initialized with oxygenated organic compounds and $\Delta NO_x/\Delta CO$ of 0.02 (S. Mason, personal communication, 2002). An important implication

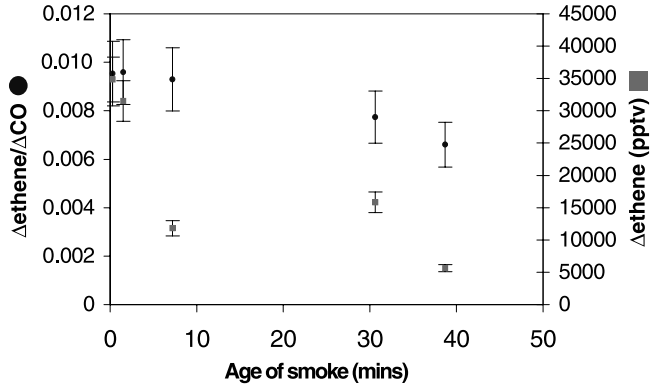

Figure 11. As for Figure 10 but for ethene.

Table 4. Excess Mixing Ratios of Species Divided by the Excess Mixing Ratio of CO for Samples 1 Through 5 in Table 1

Species	Sample 2	Sample 1	Sample 3	Sample 4	Sample 5	Uncertainty of Each Sample, %
			Gases, ppbv/ppmv of CO			
Sulfur dioxide (SO_2)	6.8	20	12	4.6	10	12
Methane (CH_4)	44	38	39	38	40	10
Dimethyl sulfide (C_2H_6S)	1.2×10^{-2}	8.6×10^{-3}	9.2×10^{-3}	6.8×10^{-3}	6.0×10^{-3}	14
Methyl bromide (CH_3Br)	6.6×10^{-2}	6.1×10^{-3}	7.4×10^{-3}	6.5×10^{-3}	5.4×10^{-3}	14
Methyl chloride (CH_3Cl)	0.75	0.71	0.78	0.70	0.59	14
Methyl iodide (CH_3I)	1.2×10^{-2}	8.6×10^{-3}	9.2×10^{-3}	6.8×10^{-3}	6.0×10^{-3}	14
Methyl nitrate (CH_3ONO_2)	6.6×10^{-3}	6.1×10^{-3}	7.4×10^{-3}	6.5×10^{-3}	5.4×10^{-3}	14
Ethane (C_2H_6)	3.3	2.7	2.7	3.1	2.9	14
Ethene (C_2H_4)	9.5	9.6	9.3	7.7	6.6	14
Propane (C_3H_8)	0.59	0.46	0.48	0.55	0.52	14
Propene (C_3H_6)	2.4	2.3	2.0	1.1	0.94	14
Acetylene (C_2H_2)	3.2	3.5	3.4	3.3	3.1	14
i-butane (C_4H_{10})	4.5×10^{-2}	3.9×10^{-2}	3.5×10^{-2}	3.7×10^{-2}	4.1×10^{-2}	14
n-butane (C_4H_{10})	0.12	0.10	0.10	0.11	0.10	14
t-2-butene (C_4H_8)	1.2×10^{-1}	9.3×10^{-2}	6.2×10^{-2}	4.7×10^{-2}	5.9×10^{-3}	14
1-butene (C_4H_8)	0.34	0.31	0.26	0.12	8.65×10^{-2}	14
c-2-butene (C_4H_8)	8.5×10^{-2}	6.9×10^{-2}	5.0×10^{-2}	2.7×10^{-2}	7.0×10^{-3}	14
i-pentane (C_5H_{12})	1.3×10^{-2}	9.4×10^{-3}	1.0×10^{-2}	1.2×10^{-2}	7.0×10^{-3}	14
n-pentane (C_5H_{12})	2.9×10^{-2}	2.2×10^{-2}	2.2×10^{-2}	2.5×10^{-2}	2.0×10^{-2}	14
1,3-butadiene (C_4H_6)	3.9×10^{-1}	3.6×10^{-1}	3.0×10^{-1}	4.2×10^{-2}	3.9×10^{-2}	14
3-methyl-1-butene (C_5H_{10})	3.5×10^{-2}	3.2×10^{-2}	2.8×10^{-2}	1.5×10^{-2}	1.2×10^{-2}	14
t-2-pentene (C_5H_{10})	2.9×10^{-2}	2.6×10^{-2}	1.8×10^{-2}	bdl	bdl	14
2-methyl-2-butene (C_5H_{10})	3.4×10^{-2}	2.7×10^{-2}	1.5×10^{-2}	bdl	bdl	14
2-methyl-1-butene (C_5H_{10})	3.6×10^{-2}	3.4×10^{-2}	2.4×10^{-2}	6.4×10^{-3}	5.9×10^{-3}	14
c-2-pentene (C_5H_{10})	1.8×10^{-2}	1.6×10^{-2}	1.1×10^{-2}	bdl	bdl	14
n-hexane (C_6H_{14})	5.9×10^{-2}	5.4×10^{-2}	4.7×10^{-2}	2.9×10^{-2}	2.3×10^{-2}	14
Isoprene (C_5H_8)	0.21	0.19	0.10	0	-3.5×10^{-3}	14
2-methyl-1-pentene (C_6H_{12})	2.1×10^{-2}	1.7×10^{-2}	1.3×10^{-2}	bdl	bdl	14
Heptane (C_7H_{16})	2.9×10^{-2}	1.8×10^{-2}	9.4×10^{-3}	3.9×10^{-3}	-4.7×10^{-3}	14
Benzene (C_6H_6)	0.99	0.92	0.89	0.86	0.74	14
Toluene (C_7H_8)	0.84	0.64	0.63	0.62	0.45	14
			Particulates, μg m^{-3}/ppmv of CO			
Total particulate matter (TPM)	-	350	198	-	174	10
Organic carbon (OC)	-	62	42	-	36	10
Black carbon (BC)	-	10.5	5.6	-	7.2	10
Chloride (Cl^-)	-	59	22	-	6.3	10
Nitrate (NO_3^-)	-	3.9	5.0	-	9.7	11
Sulfate (SO_4^{2-})	-	7.2	6.3	-	8.1	11
Potassium (K^+)	-	21	6.9	-	3.6	11

of the high average OH concentration that we have derived from the Timbavati plume is that the lifetime of reactive species in biomass-burning plumes is much shorter than suggested by 24-h average lifetimes calculated for ambient conditions.

[48] The short lifetimes of many fire emissions are evident in the data for the Timbavati fire (Table 4). For example, Δ1-butene/ΔCO decreased to 35% of its initial value in 31 min; much faster than implied by the average tropical lifetime of 2.2 h calculated by *Mauzerall et al.* [1998] using a 24-hour average OH concentration of 2.7×10^6 molecules cm^{-3}. The Δisoprene/ΔCO ratio fell by a factor of 2 in only 7 min, and $\Delta C_2H_4/\Delta CO$ fell by 30% in 39 min. These changes are also much faster than implied by

Table 5. Excess Mixing Ratio Divided by the Excess Mixing Ratio of CO (in Units of ppbv/ppmv CO) for Chemical Species for Samples (a) Through (k) in Table 1

Species	Sample b	a	d	h	c	e	f	g	i	j	k
Methane (CH_4)	53	60	88	42	61	52	72	63	60	43	49
Ethene (C_2H_4)	14	16	13	13	12	bdl	bdl	bdl	bdl	bdl	bdl
Acetylene (C_2H_2)	3	3	bdl	bdl	3	bdl	bdl	bdl	bdl	bdl	bdl
Formaldehyde (HCHO)	18	19	22	16	9	30	23	32	18	16	47
Methanol (CH_3OH)	14	15	22	12	16	9	bdl	8	bdl	13	13
Acetic Acid (CH_3COOH)	14	13	25	34	8	29	43	38	49	55	76
Formic Acid (HCOOH)	8	6	bdl	4	10	10	bdl	5	bdl	bdl	bdl
Ammonia (NH_3)	3	1	bdl	2	bdl	bdl	bdl	bdl	bdl	bdl	bdl
Nitric oxide (NO)	13	10	bdl	bdl	bdl	bdl	bdl	bdl	bdl	bdl	bdl
Nitrogen dioxide (NO_2)	31	24	bdl	32	29	bdl	bdl	bdl	11	bdl	bdl
Hydrogen cyanide (HCN)	7	6	10	bdl	10	8	11	12	bdl	bdl	bdl
Ozone (O_3)	−13	−9	13	bdl	12	57	60	90	57	84	46

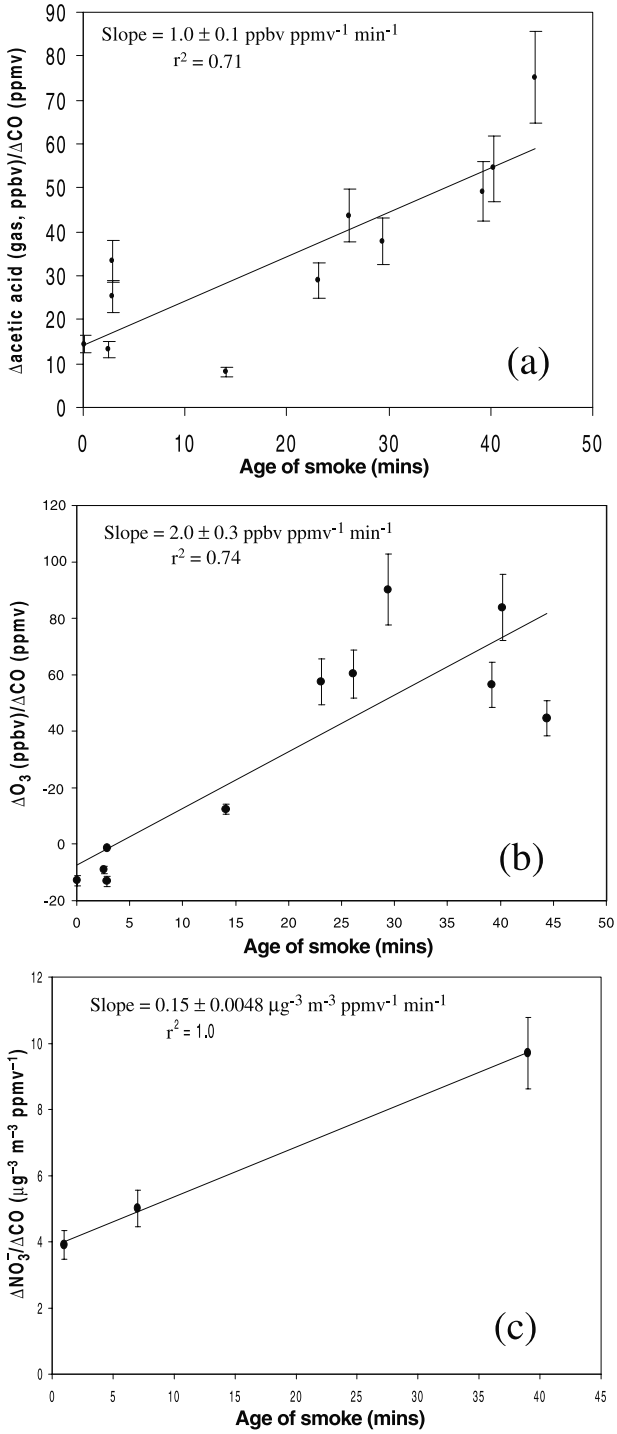

Figure 12. Excess mixing ratios normalized with respect to CO as a function of age of smoke in the Timbavati plume of (a) acetic acid and (b) ozone. The ratio of particulate nitrate (in $\mu g\ m^{-3}$) normalized by the excess volume mixing ratio of CO (in ppmv) is shown in (c).

the lifetimes calculated by *Mauzerall et al.* [1998] of 1 and 12 h, respectively.

[49] We conclude that the photochemical environment in young biomass burning plumes differs considerably from ambient or average conditions and requires specialized study, particularly as these young plumes are a major global source of trace gases and particles.

6.3.4. Transformations of Particles

[50] The concentrations of CN and accumulation-mode particles (0.1–3 μm diameter) changed as the smoke from the Timbavati fire aged.

[51] Figure 17a shows the excess CN concentrations measured as the Convair-580 flew along the length of the plume between 0950 and 0955 UTC. The concentrations were high (~500,000 cm^{-3}) in the immediate vicinity of the fire but fell off sharply (to 50,000 cm^{-3}) within about 5.5 km and remained near this value to about 23 km downwind. However, even at 23 km downwind the excess CN concentrations were well over an order of magnitude greater than in the ambient air. To compensate for the effects of plume dilution on the excess CN concentrations, we show in Figure 17b ΔCN/ΔCO along the length of the plume. The normalized excess CN concentrations decrease for about 10 min, but thereafter show an overall increase with aging. We attribute the initial decrease to coagulation of the highly concentrated particles. If we assume monodispersed particles with a diameter of 0.01 μm, the estimated e-folding time for decreasing CN concentrations by particle coagulation is ~9 min up to about 3 km from the fire, but at ~20 km from the fire it is ~170 min. Changing the diameter of the assumed monodispersed particles to 0.003 and 0.1 μm changes the e-folding time up to 3 km from the fire to 2.5 and 70 min, respectively. The increase in the normalized excess CN concentrations beyond ~10 min, seen in Figure 17b, could be due to gas-to-particle (g-to-p) conversion dominating over coagulation. The production of new particles by g-to-p conversion, as opposed to condensation onto

Table 6. Slope, Standard Error of Slope, and Correlation Coefficient (r^2) From Regression of Excess Mixing Ratio of Species Divided by Excess Mixing Ratio of CO Versus Age of Smoke[a]

Species	Slope ± Standard Error of Slope	r^2
Species for Which ΔX/ΔCO Increased Significantly as Smoke Aged Over ~40–45 min		
Nitrate (NO_3^-)	0.15 ± 0.0048 μg m^{-3} $ppmv^{-1}$ min^{-1}	1.0
Ozone (O_3)	2.0 ± 0.3 ppbv $ppmv^{-1}$ min^{-1}	0.74
Acetic acid (CH_3CO_2H)	1.0 ± 0.1 ppbv $ppmv^{-1}$ min^{-1}	0.71
Species for Which ΔX/ΔCO Decreased Significantly as Smoke Aged Over ~40–45 min, ppbv $ppmv^{-1}min^{-1}$		
Nitrogen dioxide (NO_2)	$(-4.7 \pm 1.4) \times 10^{-1}$	0.79
Ethene (C_2H_4)	$(-7.2 \pm 0.7) \times 10^{-2}$	0.97
Propene (C_3H_6)	$(-3.7 \pm 0.2) \times 10^{-2}$	0.99
t-2-pentene (C_5H_{10})	$(-7.5 \pm 0.9) \times 10^{-4}$	0.96
2-methyl-2-butene (C_5H_{10})	$(-8.0 \pm 1.7) \times 10^{-4}$	0.88
c-2-pentene (C_5H_{10})	$(-4.6 \pm 0.6) \times 10^{-4}$	0.95
2-methyl-1-pentene (C_6H_{12})	$(-5.2 \pm 0.7) \times 10^{-4}$	0.95
1,3-butadiene (C_4H_6)	$(-9.4 \pm 0.9) \times 10^{-3}$	0.97
1-butene (C_4H_8)	$(-6.2 \pm 0.5) \times 10^{-3}$	0.98
Isoprene (C_5H_8)	$(-5.3 \pm 1.0) \times 10^{-3}$	0.91
Benzene (C_6H_6)	$(-4.5 \pm 1.3) \times 10^{-3}$	0.80
t-2-butene (C_4H_8)	$(-2.2 \pm 0.6) \times 10^{-3}$	0.84
c-2-butene (C_4H_8)	$(-1.7 \pm 0.3) \times 10^{-3}$	0.92
n-hexane (C_6H_{14})	$(-8.6 \pm 0.7) \times 10^{-4}$	0.98
2-methyl-1-butene (C_5H_{10})	$(-7.8 \pm 1.0) \times 10^{-4}$	0.95
n-heptane (C_7H_{16})	$(-6.4 \pm 1.8) \times 10^{-4}$	0.81
3-methyl-1-butene (C_5H_{10})	$(-5.6 \pm 0.4) \times 10^{-4}$	0.99

[a]See Tables 2 and 3 for measurement techniques. "Significant" refers to a statistical confidence level = 95%.

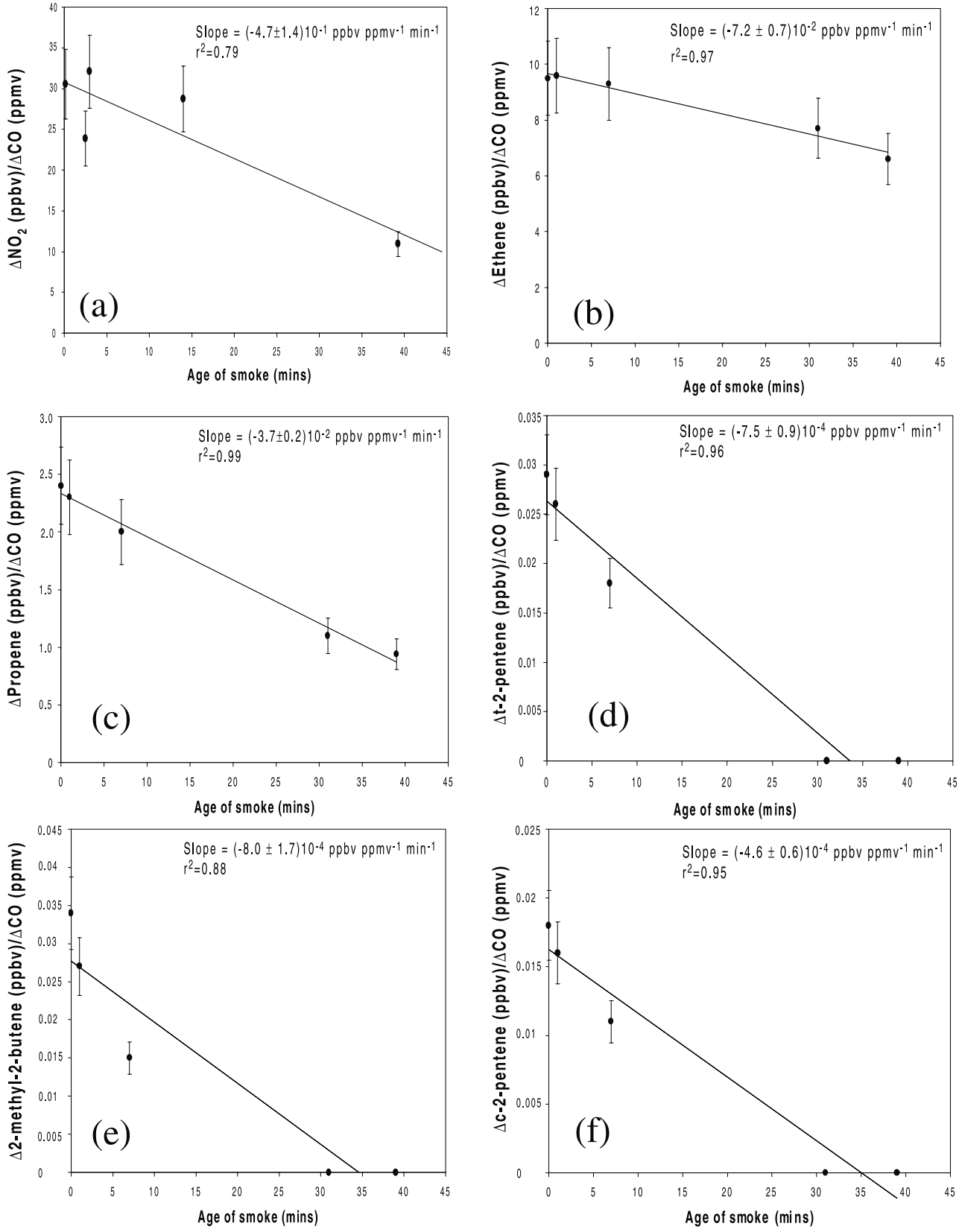

Figure 13. As for Figure 12 but for (a) nitrogen dioxide (NO_2), (b) ethene (C_2H_4), (c) propene (C_3H_6), (d) *t*-2-pentene (C_5H_{10}), (e) 2-methyl-2-butene (C_5H_{10}), and (f) *c*-2-pentene (C_5H_{10}).

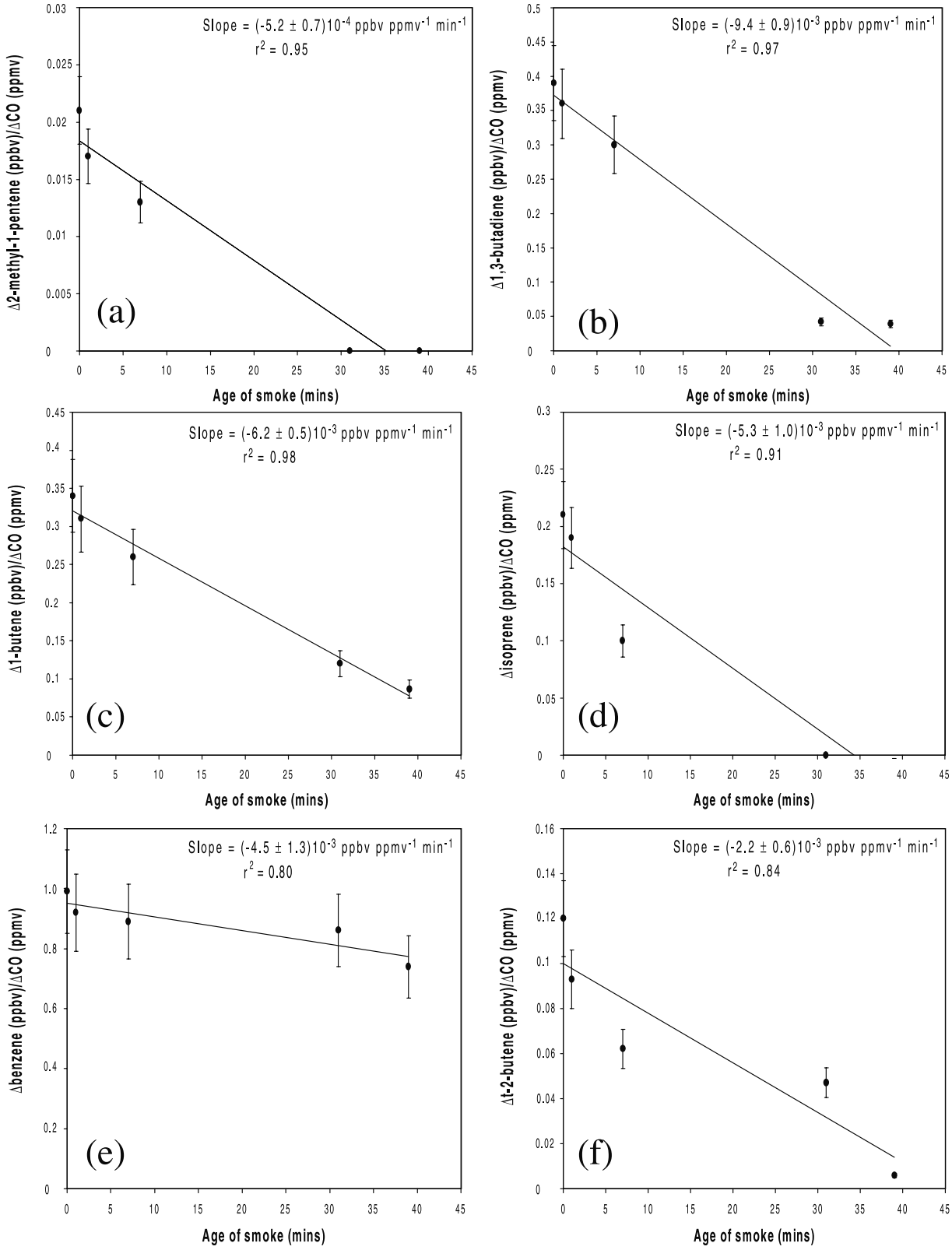

Figure 14. As for Figure 12 but for (a) 2-methyl-1-pentene (C_6H_{12}), (b) 1,3-butadiene (C_4H_6), (c) 1-butene (C_4H_8), (d) isoprene (C_5H_8), (e) benzene (C_6H_6), and (f) *t*-2-butene (C_4H_8).

existing particles, is favored by smaller surface area concentrations of particles; the aerosol surface area concentration in the Timbavati plume decreased by a factor of about five from 0 to 10 km downwind of the fire. Discussions by *Gao et al.* [2003] on g-to-p conversion of some organic species support this interpretation.

[52] Shown in Figure 18 are particle size distributions, measured with the TSI 3320 aerodynamic particle sizer, for

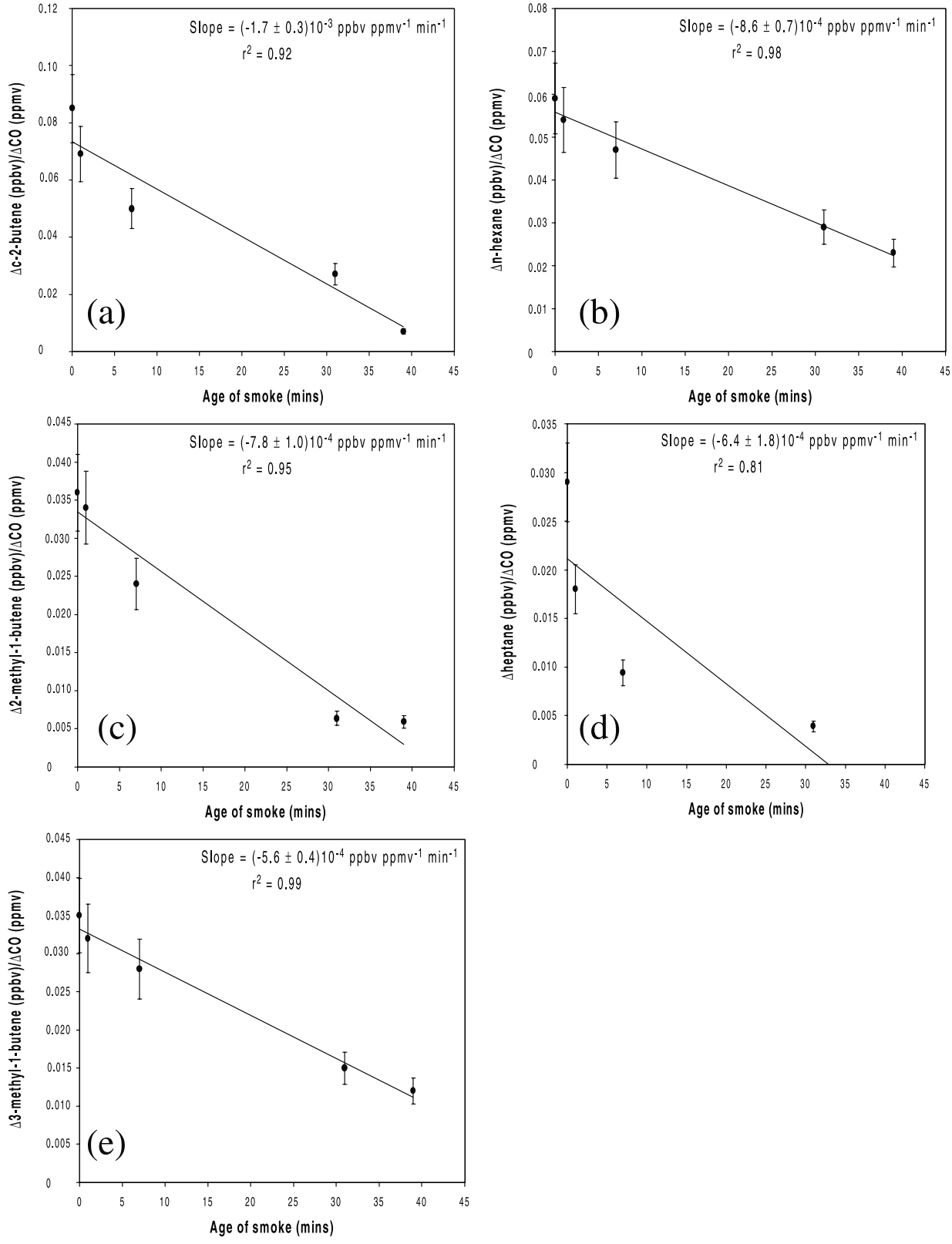

Figure 15. As for Figure 12 but for (a) *c*-2-butene (C_4H_8), (b) *n*-hexane (C_6H_{14}), (c) 2-methyl-1-butene (C_5H_{10}), (d) heptane (C_7H_{16}), and (e) 3-methyl-1-butene (C_5H_{10}).

smoke samples 0 and 39 min old in the Timbavati plume. The effects of dilution on the particle concentrations due to mixing with the ambient air have been removed from the curves shown in Figure 18 by dividing the concentrations by CO. For particles less than about 1.5 μm in diameter, the particle concentrations decreased as the smoke aged, whereas for larger particles the concentrations were greater in the smoke that was 39 min old than in the smoke

Table 7. Estimates of Average OH Concentrations in the Timbavati Plume During the First ~40 min of Smoke Aging[a]

Pair	[OH] From Slope of Plot, molecules cm^{-3}	Correlation Coefficient (r^2)	Percentage Loss of Alkene by O_3	[OH] Corrected for Loss by O_3, molecules cm^{-3}
Propene/ethene	1.5×10^7	0.98	-	1.5×10^7
1-butene/ethene	1.8×10^7	0.99	-	1.8×10^7
Ethene/ethane	1.8×10^7	0.74	3.2	1.8×10^7
Ethene/CO	1.9×10^7	0.97	3.2	1.9×10^7
Propene/ethane	1.6×10^7	0.96	6.6	1.5×10^7
Propene/CO	1.6×10^7	1.00	6.6	1.5×10^7
1-butene/ethane	1.8×10^7	0.99	4.9	1.7×10^7
1-butene/CO	1.9×10^7	0.99	4.9	1.8×10^7
Average	$(1.7 \pm 0.2) \times 10^7$	-	-	$(1.7 \pm 0.2) \times 10^7$

[a]Rate coefficients for the reactions were taken from *Finlayson-Pitts and Pitts* [2000].

initially emitted from the fire. These results are consistent with the smaller particles coagulating to form the larger particles.

[53] Sample 5 (see Table 1) was the oldest sample (39 min) for which both the excess mixing ratio of CO and the excess mass of particulate nitrate were measured. From the data in Table 2, we can compute the excess mass of nitrate (per m^3 of the smoke) in sample 5, which can then be converted to the number of excess NO_3^- molecules per cubic meter of smoke (8×10^{16}) using the molecular mass of nitrate (62) and Avogadro's number (6.022×10^{23} molecules mol^{-1}). We can also compute the number of excess CO molecules per cubic meter of smoke in sample 5 (2×10^{19}) from its excess volume-mixing ratio of 0.88 ppmv. These calculations imply that the ratio of excess NO_3^- molecules to excess CO molecules in sample 5 is ~0.004. This ratio is higher than the initial $\Delta NH_3/\Delta CO$ ratio in the smoke (~0.002; see Table 5 samples a and b).

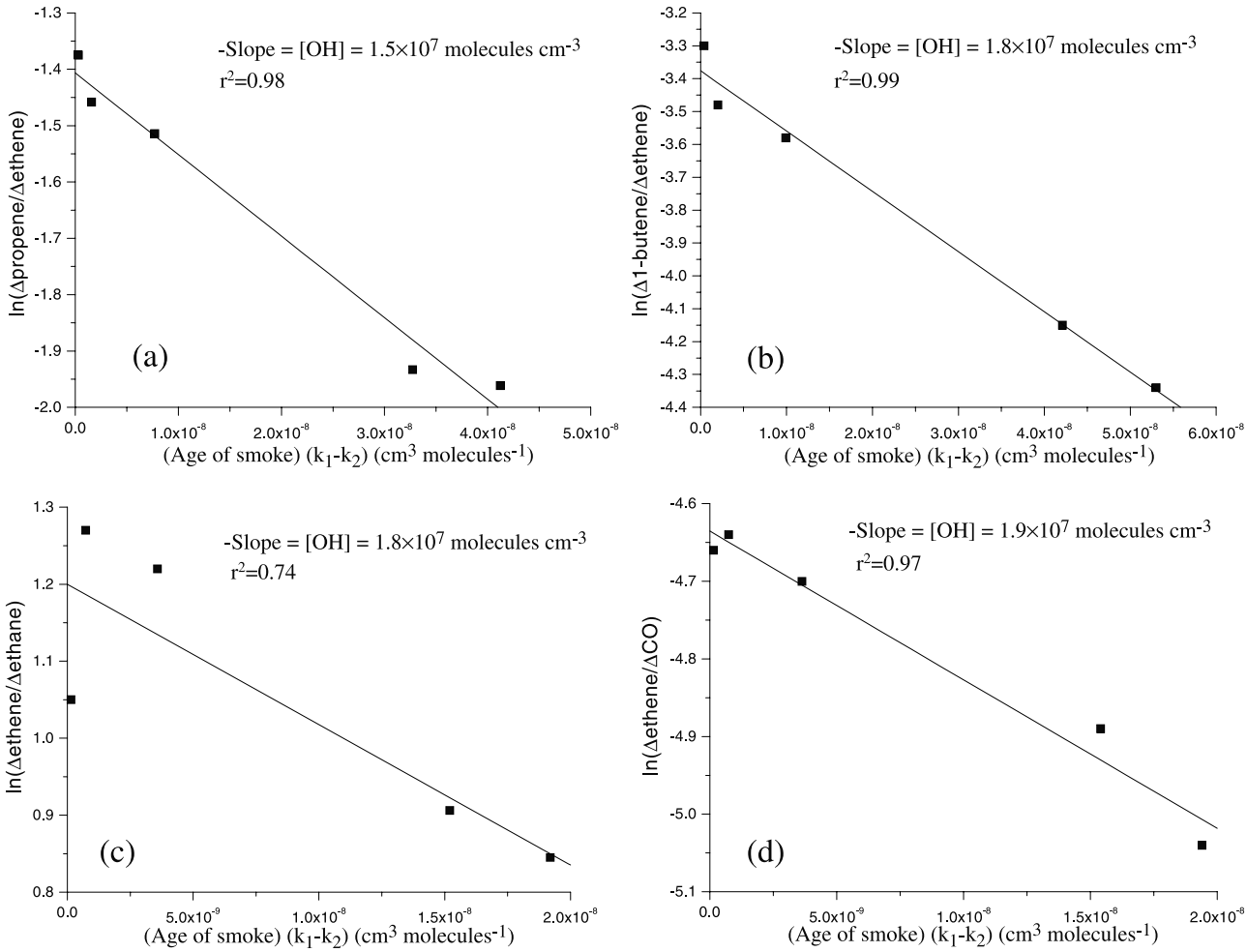

Figure 16. Plots of equation (5) based on measurements in the Timbavati plume. The slope provides an estimate of the average OH concentration in the plume during the first ~40 min of smoke aging.

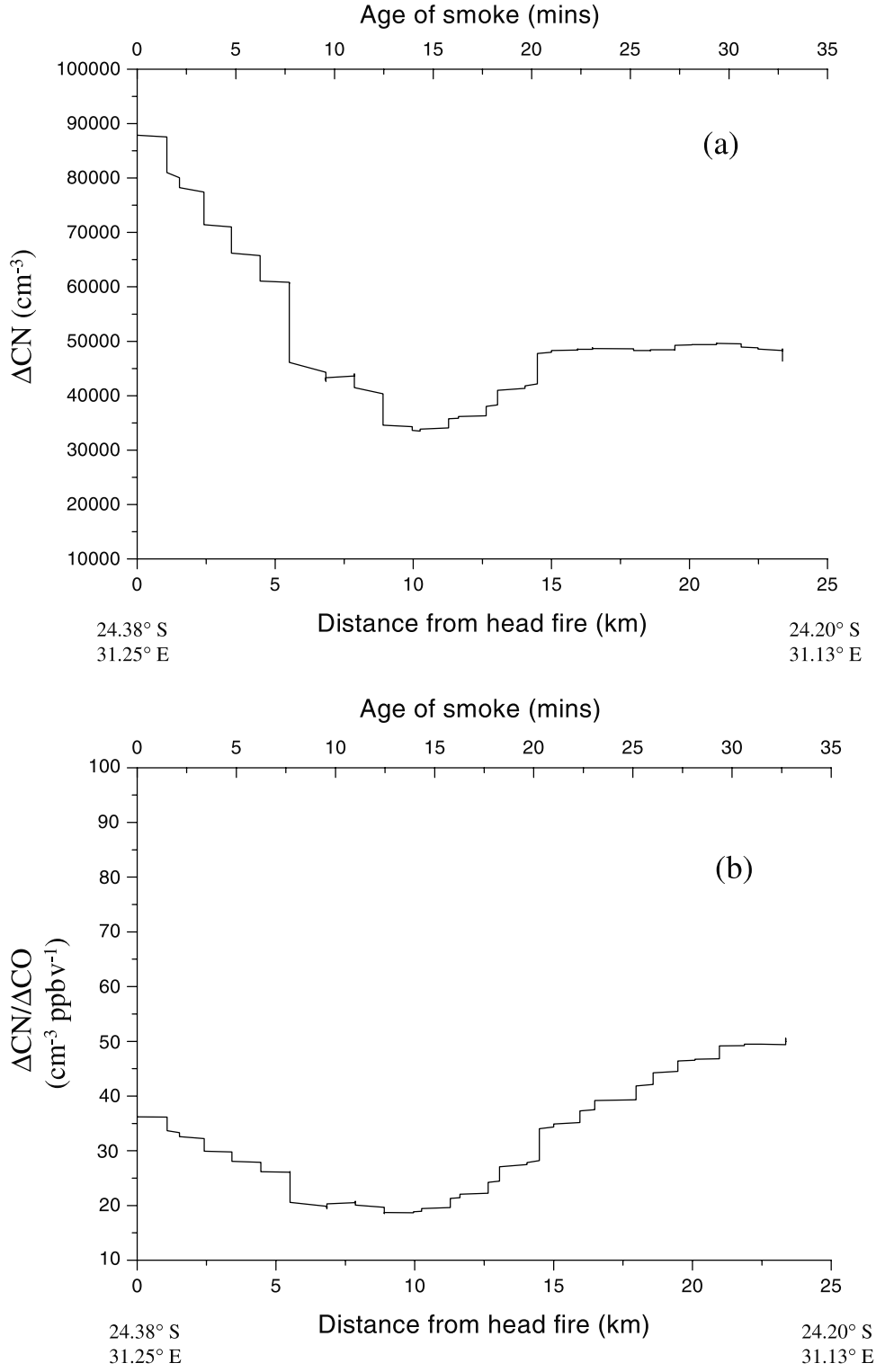

Figure 17. (a) Running mean concentration of condensation nuclei (CN) along the length of the Timbavati smoke plume. (b) Excess concentration of CN normalized by excess concentration of CO along the length of the Timbavati smoke plume. The ambient concentration of CN was $\sim$1000 cm^{-3}. The excess concentrations of CO were obtained by interpolating canister measurements.

Therefore, not all of the nitrate can be present as ammonium nitrate. This suggests that some of the NO_3^- may be paired with K^+ or other positive ions rather than ammonium (NH_4^+). Potassium nitrate was observed in older smoke samples by *Li et al.* [2003] using electron microscopy. The $\Delta NO_3^-/\Delta CO$ ratio of 0.004 for sample 5 can also be compared to the initial $\Delta NO_x/\Delta CO$ ratio (see Table 5 samples a and b) of $\sim$0.04. The comparison

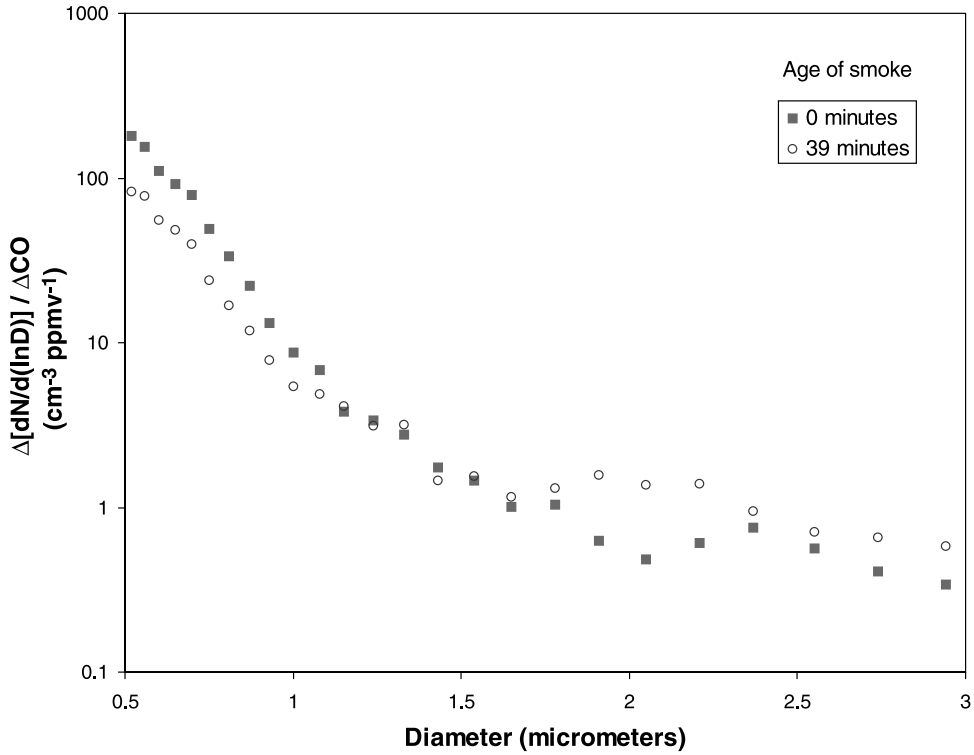

Figure 18. Aerosol size distributions of smoke over fire (0 min) and after aging for 39 min. The excess particle concentrations are divided by excess CO concentrations to eliminate the effects of mixing of the smoke with the ambient air.

implies that up to ~10% of the initial NO_x was converted to particle nitrate in ~40 min. Much of the rest of the NO_x was probably converted to gas-phase reservoir species, such as PAN, HNO_3(g), alkyl nitrates, etc. (In extratropical fires, the initial $\Delta NH_3/\Delta CO$ and $\Delta NO_x/\Delta CO$ ratios are more nearly equal, which may favor the production of relatively more particle ammonium nitrate [*Goode et al.*, 2000].) A similar analysis for sulfur species suggests that ~10% of the initial SO_2 was converted to SO_4^{2-} in ~40 min.

[54] Four papers in this Special Issue of *Journal of Geophysical Research* provide additional information on the effects of aging on particles in the plume from the Timbavati fire. *Magi and Hobbs* [2003] show that the change in the light-scattering coefficient of the smoke, as the relative humidity was increased from 30 to 80%, was less for smoke aged over 40 min than for smoke just over the fire. Transmission electron microscopy (TEM) was used to study individual particles in the smoke from the Timbavati fire [*Li et al.*, 2003; *Pósfai et al.*, 2003]. In the initial smoke just above the fire, potassium chloride (KCl) particles with organic coatings dominated, with lesser amounts of calcium-bearing particles, tar balls, organic particles, sea salt, mineral dust, and minor amounts of soot. The most obvious effect of aging of the smoke was a transformation from KCl particles to potassium sulfate and nitrate particles. The relative number concentration of organic particles was largest in the young smoke, whereas tar balls were dominant in the more aged smoke. *Gao et al.* [2003] discuss the secondary formation of inorganic and organic species in smoke from the Timbavati and other fires. It was found that secondary formation of sulfate, nitrate, levoglucosan, and several organic acids occurred during the initial aging of smoke aerosols, presumably due to condensation.

7. Conclusions

[55] In this paper we have described airborne measurements of the emissions and initial evolution of particles and gases from a 1000-ha prescribed burn of savanna vegetation in South Africa. These measurements represent the most extensive and quantitative data yet reported on the effects of aging on biomass smoke.

[56] This study has provided:

1. Excess mixing ratios and downwind changes in normalized excess mixing ratios for 42 trace gases, total particulate matter, organic carbon, black carbon, and particulate Cl^-, NO_3^-, SO_4^{2-} and K^+ (Tables 2–5).
2. An estimate of the average OH concentration in the young smoke plume (Table 7 and Figure 16).
3. Downwelling and upwelling UV fluxes (300–390 nm) within the smoke along the length of the plume (Table 1 and Figure 7), and the spectral depletion of solar radiation by the smoke (Figures 8 and 9).
4. Measurements of the light-scattering coefficient, and condensation nucleus (CN) concentrations across the width of the smoke plume at various distances downwind of the fire (Figures 5 and 6), CN measurements along the length of the plume (Figure 17), and the evolution of the particle size spectra during ~40 min of aging (Figure 18).

[57] Some of the principal conclusions from these measurements are:

1. The CO-normalized excess mixing ratios of nitrate, ozone, and gaseous acetic acid increased significantly as the smoke aged over ~40–45 min, indicating that these species were produced by chemical reactions in the plume (Tables 4–6 and Figure 12).

2. The CO-normalized excess mixing ratio of seventeen species decreased significantly as the smoke aged over ~40–45 min, indicating that they were consumed by chemical reactions (Tables 4–6 and Figures 13–15).

3. The downwelling UV flux near the center of the smoke plume was about two-thirds of that near the top of the plume. Despite this, the average OH concentration in the relatively young smoke, estimated to be $(1.7 \pm 0.2) \times 10^7$ molecules cm^{-3}, was high enough to significantly shorten the lifetimes of reactive species.

4. The transformations of species in the smoke were faster than observed in extratropical regions.

5. The CO-normalized excess CN concentrations decreased during the first ~10 min of aging and thereafter increased (Figure 17). We attribute this to particle coagulation initially dominating gas-to-particle conversion, and then vice versa at longer times.

6. The CO-normalized concentrations of particles <1.5 μm diameter decreased as the smoke aged over ~40 min, whereas, for larger particles, the concentrations were greater in the aged smoke (Figure 18).

[58] **Acknowledgments.** We thank all members of the UW-CARG for help in obtaining measurements, Tobias Landmann for ground characterization of the fire site, and Brook Jilek for help in initial data analysis. This research was supported by grants NAG5-9022 and NAG5-7675 from NASA's Radiation Science Program and grant ATM-9901624 from NSF's Division of Atmospheric Sciences, and is part of the SAFARI 2000 Southern African Regional Science Initiative.

References

Andreae, M. O., B. E. Anderson, D. R. Blake, J. D. Bradshaw, J. E. Collins, G. L. Gregory, G. W. Sachse, and M. C. Shipman, Influence of plumes from biomass burning on atmospheric chemistry over the equatorial and tropical Atlantic during CITE 3, *J. Geophys. Res.*, *99*, 12,793–12,808, 1994.

Andreae, M. O., E. Atlas, H. Cachier, W. R. Cofer III, G. W. Harris, G. Helhas, R. Koppmann, J. Lacaux, and D. Ward, Trace gas and aerosol emissions from savanna fires, in *Biomass Burning and Global Change*, edited by J. S. Levine, pp. 278–295, MIT Press, Cambridge, Mass., 1996.

Bergstrom, R., P. B. Russell, and P. Hignett, Wavelength dependence of the absorption of black carbon particles: Predictions and results from the TARFOX experiment and implications for the aerosol single-scattering albedo, *J. Atmos. Sci.*, *59*, 567–577, 2002.

Bergstrom, R., P. Pilewskie, B. Schmid, and P. B. Russell, Estimates of the spectral aerosol single scattering albedo and aerosol radiative effects during SAFARI 2000, *J. Geophys. Res.*, *108*, doi:10.1029/2002JD002435, in press, 2003.

Colman, J. J., A. L. Swanson, S. Meinardi, B. C. Sive, D. R. Blake, and F. S. Rowland, Description of the analysis of a wide range of volatile organic compounds in whole air samples collected during PEM-Tropics A and B, *Anal. Chem.*, *73*, 3723–3731, 2001.

Crutzen, P. J., and M. O. Andreae, Biomass burning in the tropics: Impact on atmospheric chemistry and biogeochemical cycles, *Science*, *250*, 1669–1678, 1990.

Delmas, R., On the emissions of carbon, nitrogen and sulfur in the atmosphere during bushfires in intertropical savannah zones, *Geophys. Res. Lett.*, *9*, 761–764, 1982.

Eagan, R. C., P. V. Hobbs, and L. F. Radke, Measurements of cloud condensation nuclei and cloud droplet size distributions in the vicinity of forest fires, *J. Appl. Meteorol.*, *13*, 553–557, 1974.

Ferek, R. J., J. S. Reid, P. V. Hobbs, D. R. Blake, and C. Liousse, Emission factors of hydrocarbons, halocarbons, trace gases, and particles from biomass burning in Brazil, *J. Geophys. Res.*, *103*, 32,107–32,118, 1998.

Finlayson-Pitts, B. J., and J. W. Pitts Jr., *Chemistry of the Upper and Lower Atmosphere*, Academic, San Diego, Calif., 2000.

Fishman, J., K. Fakhruzzaman, B. Cros, and D. Nganga, Identification of widespread pollution in the southern hemisphere deduced from satellite analyses, *Science*, *252*, 1693–1696, 1991.

Gao, S., D. A. Hegg, P. V. Hobbs, T. W. Kirchstetter, B. Magi, and M. Sadelik, Water-soluble organic components in aerosols associated with savanna fires in southern Africa: Identification, evolution and distribution, *J. Geophys. Res.*, *108*, doi:10.1029/2002JD002324, in press, 2003.

Goode, J. G., R. J. Yokelson, D. E. Ward, R. A. Susott, R. E. Babbitt, M. A. Davies, and W. M. Hao, Measurements of excess O_3, CO_2, CO, CH_4, C_2H_4, C_2H_2, HCN, NO NH_3, HCOOH, CH_3COOH, HCHO and CH_3OH in 1997 Alaskan biomass burning plumes by airborne Fourier transform infrared spectroscopy (AFTIR), *J. Geophys. Res.*, *105*, 22,147–22,166, 2000.

Gundel, L. A., R. L. Dod, H. Rosen, and T. Novakov, The relationship between optical attenuation and black carbon concentrations for ambient and source particles, *Sci. Total Environ.*, *36*, 197–202, 1984.

Hao, W. M., and M. H. Liu, Spatial and temporal distribution of tropical biomass burning, *Global Biochem. Cycles*, *8*, 495–503, 1994.

Hobbs, P. V., and L. F. Radke, Cloud condensation nuclei from a simulated forest fire, *Science*, *163*, 279–280, 1969.

Hobbs, P. V., J. S. Reid, J. A. Herring, J. D. Nance, R. E. Weiss, J. L. Ross, D. A. Hegg, R. D. Ottmar, and C. Liousse, Particle and trace-gas measurements in the smoke from prescribed burns of forest products in the Pacific northwest, in *Biomass Burning and Global Change*, vol. 2, edited by J. S. Levine, pp. 697–715, MIT Press, Cambridge, Mass., 1996.

Hobbs, P. V., J. S. Reid, R. A. Kotchenruther, R. J. Ferek, and R. Weiss, Direct radiative forcing by smoke from biomass burning, *Science*, *275*, 1776–1778, 1998.

Hurst, D. F., D. W. T. Griffith, J. N. Carras, D. J. Williams, and P. J. Fraser, Measurements of trace gases emitted by Australian savanna fires during the 1990 dry season, *J. Atmos. Chem.*, *18*, 33–56, 1994.

Kirchstetter, T. W., C. E. Corrigan, and T. Novakov, Laboratory and field investigation of the adsorption of gaseous organic compounds onto quartz filters, *Atmos. Environ.*, *35*, 1663–1671, 2001.

Kirchstetter, T. W., T. Novakov, P. V. Hobbs, and B. Magi, Airborne measurements of carbonaceous aerosols in southern Africa during the dry, biomass burning season, *J. Geophys. Res.*, *108*, doi:10.1029/2002JD002171, in press, 2003.

Li, J., M. Pósfai, P. V. Hobbs, and P. R. Buseck, Individual aerosol particles from biomass burning in southern Africa: 2. Compositions and aging of inorganic particles, *J. Geophys. Res.*, *108*, doi:10.1029/2002JD002310, in press, 2003.

Liousse, C., C. Devaux, F. Dulac, and H. Cachier, Aging of savanna biomass aerosols: Consequences on their optical properties, *J. Atmos. Chem.*, *22*, 1–17, 1995.

Logan, J. A., M. J. Prather, S. C. Wofsy, and M. B. McElroy, Tropospheric chemistry: A global perspective, *J. Geophys. Res.*, *86*, 7210–7254, 1981.

Magi, B. I., and P. V. Hobbs, The effects of humidity on aerosols in southern Africa during the biomass burning season, *J. Geophys. Res.*, *108*, doi:10.1029/2002JD002144, in press, 2003.

Mason, S. A., R. J. Field, R. J. Yokelson, M. A. Kochivar, M. R. Tinsley, D. A. Ward, and W. M. Hao, Complex effects arising in smoke plume simulations due to inclusion of direct emissions of oxygenated organic species from biomass combustion, *J. Geophys. Res.*, *106*, 12,527–12,539, 2001.

Mauzerall, D. L., D. J. Jacob, S.-M. Fan, J. D. Bradshaw, G. L. Gregory, G. W. Sachse, and D. R. Blake, Origin of tropospheric ozone at remote high northern latitudes in summer, *J. Geophys. Res.*, *101*, 4175–4188, 1996.

Mauzerall, D. L., J. A. Logan, D. J. Jacob, B. E. Anderson, D. R. Blake, J. D. Bradshaw, B. Heikes, G. W. Sachse, H. Singh, and B. Talbot, Photochemistry in biomass burning plumes and implications for tropospheric ozone over the tropical South Atlantic, *J. Geophys. Res.*, *103*, 8401–8423, 1998.

Novakov, T., Microchemical characterization of aerosols, in *Nature, Aim and Methods of Microchemistry*, edited by H. Malissa, M. Grasserbaure, and R. Belcher, pp. 141–165, Springer-Verlag, New York, 1981.

Novakov, T., Soot in the atmosphere, in *Particulate Carbon: Atmospheric Life Cycle*, edited by G. T. Wolff and R. L. Klimish, pp. 19–41, Plenum, New York, 1982.

Pilewskie, P., J. Pommier, R. Bergstrom, W. Gore, S. Howard, M. Rabbette, B. Schmid, S.-C. Tsay, and P. V. Hobbs, Solar spectral radiative forcing by aerosols during SAFARI 2000, *J. Geophys. Res.*, *108*, doi:10.1029/2002JD002411, in press, 2003.

Pósfai, M., R. Simonics, J. Li, P. V. Hobbs, and P. R. Buseck, Individual aerosol particles from biomass burning in southern Africa: 1. Composi-

tions and size distributions of carbonaceous particles, *J. Geophys. Res.*, *108*, doi:10.1029/2002JD002291, in press, 2003.
Radke, L. F., J. L. Stith, D. A. Hegg, and P. V. Hobbs, Airborne studies of particles and gases from forest fires, *J. Air Pollut. Control Assoc.*, *28*, 30–34, 1978.
Radke, L. F., D. A. Hegg, J. H. Lyons, C. A. Brock, P. V. Hobbs, R. Weiss, and R. Rasmussen, Airborne measurements on smokes from biomass burning, in *Aerosols and Climate*, edited by P. V. Hobbs and M. P. McCormick, pp. 411–422, A. Deepak Pub., Hampton, Va., 1988.
Reid, J. S., P. V. Hobbs, R. J. Ferek, D. R. Blake, J. V. Martins, M. R. Dunlap, and C. Liousse, Physical, chemical, and optical properties of regional hazes dominated by smoke in Brazil, *J. Geophys. Res.*, *103*, 32,059–32,080, 1998.
Reid, J. S., T. F. Eck, S. A. Christopher, P. V. Hobbs, and B. Holben, Use of the Angstrom exponent to estimate the variability of optical and physical properties of aging smoke particles in Brazil, *J. Geophys. Res.*, *104*, 27,473–27,489, 1999.
Rosen, H., and T. Novakov, Optical-transmission through aerosol deposits on diffusely reflective filters—A method for measuring the absorbing component of aerosol-particles, *Appl. Opt.*, *22*, 1265–1267, 1983.
Seinfeld, J. H., and S. N. Pandis, *Atmospheric Chemistry and Physics*, John Wiley, New York, 1998.
Sinha, P., P. V. Hobbs, R. J. Yokelson, I. T. Bertschi, D. R. Blake, I. J. Simpson, S. Gao, T. W. Kirchstetter, and T. Novakov, Emissions of trace gases and particles from biomass burning in southern Africa, *J. Geophys. Res.*, *108*, doi:10.1029/2002JD002325, in press, 2003.
Stith, J. L., L. F. Radke, and P. V. Hobbs, Particle emissions and the production of ozone and nitrogen oxides from the burning of forest slash, *Atmos. Environ.*, *15*, 73–82, 1981.
Trentmann, J., M. O. Andreae, H.-F. Graf, P. V. Hobbs, R. D. Ottmar, and T. Trautmann, Simulation of a biomass-burning plume: Comparison of model results with observations, *J. Geophys. Res.*, *107*(D2), 4013, 10.1029/2001JD000410, 2002.
Turpin, B. J., J. J. Huntzicker, and S. V. Hering, Investigation of the organic aerosol sampling artifacts in the Los Angeles basin, *Atmos. Environ.*, *28*, 3061–3071, 1994.
Ward, D. E., and W. M. Hao, Air toxic emissions from burning of biomass globally—Preliminary estimates, paper presented at 85th Annual Meeting, Air and Waste Management Association, Vancouver, British Columbia, 1992.
Ward, D. E., and C. C. Hardy, Smoke emissions from wildland fires, *Environ. Int.*, *17*, 117–134, 1991.
Ward, D. E., and L. F. Radke, Emission measurements from vegetation fires: A comparative evaluation of methods and results, in *Fire in the Environment: The Ecological, Atmospheric and Climatic Importance of Vegetation Fires*, edited by P. J. Crutzen and J. G. Goldammer, pp. 53–76, John Wiley, New York, 1993.
White, F., *Vegetation Map of Africa*, UNESCO, Paris, 1981.
White, F., *Vegetation Map of Africa*, UNESCO, Paris, 1983.
Wofsy, S. C., et al., Atmospheric chemistry in the arctic and subarctic: Influence of natural fires, industrial emissions, and stratospheric inputs, *J. Geophys. Res.*, *97*, 16,731–16,746, 1992.
Yokelson, R. J., D. W. T. Griffith, and D. W. Ward, Open-path Fourier transform infrared studies of large-scale laboratory biomass fires, *J. Geophys. Res.*, *101*, 21,067–21,080, 1996.
Yokelson, R. J., I. T. Bertschi, T. J. Christian, P. V. Hobbs, D. E. Ward, and W. M. Hao, Trace gas measurements in nascent, aged, and cloud-processed smoke from African savanna fires by airborne Fourier transform infrared spectroscopy(AFTIR), *J. Geophys. Res.*, *108*, doi:10.1029/2002JD002322, in press, 2003.

D. R. Blake, Department of Chemistry, University of California, Irvine, CA, USA.
T. J. Christian and R. J. Yokelson, Department of Chemistry, University of Montana, Missoula, USA.
S. Gao, Department of Chemistry, University of Washington, Seattle, WA, USA.
P. V. Hobbs and P. Sinha, Department of Atmospheric Sciences, University of Washington, Seattle, WA, USA. (phobbs@atmos.washington.edu)
T. W. Kirchstetter and T. Novakov, Lawrence Berkeley National Laboratory, Berkeley, CA, USA.
P. Pilewskie, NASA Ames Research Center, Moffett Field, CA, USA.

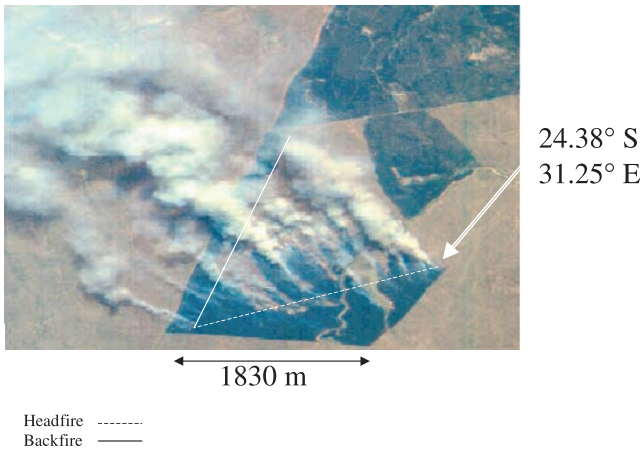

Figure 1. Nadir-viewing image at 0829 UTC on 7 September 2000 of the prescribed fire in the Timbavati Private Game Reserve obtained from AirMISR aboard the NASA ER-2 aircraft. The image is a composite constructed from red (672 nm), green (558 nm), and blue (446 nm) bands.

Figure 2. Photograph of the Timbavati fire taken at 0836 UTC on 7 September 2000 from the Convair-580 aircraft. (Photo: P. V. Hobbs)